

Moments of Axial-Vector GPD from Lattice QCD: Quark Helicity, Orbital Angular Momentum, and Spin-Orbit Correlation

Shohini Bhattacharya^a Krzysztof Cichy^b Martha Constantinou^c Xiang Gao^d Andreas Metz^c Joshua Miller^c Swagato Mukherjee^d Peter Petreczky^d Fernanda Steffens^e Yong Zhao^f

^a*Theoretical Division, Los Alamos National Laboratory, Los Alamos, New Mexico 87545, USA*

^b*Faculty of Physics and Astronomy, Adam Mickiewicz University, ul. Uniwersytetu Poznańskiego 2, 61-614 Poznań, Poland*

^c*Department of Physics, Temple University, Philadelphia, PA 19122 - 1801, USA*

^d*Physics Department, Brookhaven National Laboratory, Upton, New York 11973, USA*

^e*Institut für Strahlen- und Kernphysik, Rheinische Friedrich-Wilhelms-Universität Bonn, Nussallee 14-16, 53115 Bonn*

^f*Physics Division, Argonne National Laboratory, Lemont, IL 60439, USA*

ABSTRACT: In this work, we present a lattice QCD calculation of the Mellin moments of the twist-2 axial-vector generalized parton distribution (GPD), $\tilde{H}(x, \xi, t)$, at zero skewness, ξ , with multiple values of the momentum transfer, t . Our analysis employs the short-distance factorization framework on ratio-scheme renormalized quasi-GPD matrix elements. The calculations are based on an $N_f = 2 + 1 + 1$ twisted mass fermions ensemble with clover improvement, a lattice spacing of $a = 0.093$ fm, and a pion mass of $m_\pi = 260$ MeV. We consider both the iso-vector and iso-scalar cases, utilizing next-to-leading-order perturbative matching while omitting the disconnected contributions and gluon mixing in the iso-scalar case. For the first time, we determine the Mellin moments of \tilde{H} up to the fifth order. From these moments, we discuss the quark helicity and orbital angular momentum contributions to the nucleon spin, as well as the spin-orbit correlations of the quarks. Additionally, we perform a Fourier transform over the momentum transfer, which allows us to explore the spin structure in the impact-parameter space.

Contents

1	Introduction	1
2	Axial-vector GPD on the lattice	3
2.1	The definition of axial-vector GPDs	3
2.2	The axial-vector quasi GPD $\tilde{\mathcal{H}}$	4
3	Bare matrix elements and renormalization	5
3.1	Lattice setup	5
3.2	Bare matrix elements and renormalization	7
4	Mellin moments from short distance factorization	9
4.1	Short distance factorization	9
4.2	Moments from fixed z^2	10
4.3	Moments from combined fits	12
5	Insights into nucleon spin dynamics from axial vector GPD	14
5.1	Quark helicity, OAM, and spin-orbit correlations in nucleons	15
5.2	Impact-parameter-space interpretation	17
6	Conclusion	20

1 Introduction

Understanding the internal structure of hadrons, such as protons and neutrons, is a fundamental goal in modern particle and nuclear physics. Generalized parton distributions (GPDs) [1–3] have emerged as a powerful tool for probing the three-dimensional structure of hadrons. Unlike traditional parton distribution functions (PDFs), which provide information about the longitudinal momentum distribution of partons, GPDs offer a more comprehensive picture by incorporating both longitudinal momentum and transverse spatial distributions [4–7]. Therefore, GPDs bridge the gap between the spatial and momentum distributions of quarks and gluons within the nucleon.

The GPDs can be classified into different types based on their symmetry properties twist, and the polarization state of the parton/hadron [8–13]. Among these, the twist-2 axial vector GPD $\tilde{H}(x, \xi, t)$ is crucial for the understanding of the nucleon spin structure, a major challenge in hadronic physics [14, 15]. The first Mellin moment of this GPD is directly related to the quark helicity contribution to the nucleon spin and, through Ji’s spin decomposition scheme [2], provides insights into the orbital angular momentum (OAM). Additionally, it sheds light on spin-orbit correlations of quarks [16–18], offering valuable perspectives on the spin structure of the nucleon.

In principle, information on the GPDs can be obtained from experimental data for hard exclusive scattering processes such as the deeply virtual Compton scattering [2, 3, 19–21], deeply virtual meson production [22–24] and processes where additional particles are detected in the final state [25–30]. However, extracting GPDs from such data are highly non-trivial as it requires solving an inverse problem and disentangling multi-dimensional distributions from limited experimental observables [31, 32]. While much progress has been made in recent years [33–40], the field is still in its infancy. Consequently, computing GPDs from first principles using lattice QCD is well motivated, as it provides essential complementary information for constraining the GPDs.

Unfortunately, the direct simulation of GPDs is forbidden on a Euclidean lattice as they are defined through non-local light-cone correlators. Therefore, for a long time the focus has been on the Mellin moments of GPDs which can be computed through the matrix elements of local operators [41–60]. However, this method encounters difficulties in accessing higher moments due to signal decay and operator mixing under renormalization, which may be mitigated through the application of gradient flow [61, 62] or smearing [63]. Over the past few years, significant progress has been made in computing parton distributions using alternative methods [64–75], especially those motivated by the proposal of quasi-PDFs [68, 69]. Starting from boosted non-local equal-time correlators, the x -dependent parton distributions and their moments can be extracted using the framework of large momentum effective theory (LaMET) [76] or short distance factorization (SDF) [67, 71–73]. For reviews, see Refs. [76–81].

There has been a lot of progress in computing GPDs through LaMET and SDF in the past few years [82–99]. However, establishing these three-dimensional distributions with comprehensive x , ξ , and t dependence remains challenging due to the computational cost. Significant progress was made recently in reducing these costs, as originally proposed in Ref. [90]. By employing the Lorentz-covariant parametrization of matrix elements, quasi-GPDs can be constructed from Lorentz-invariant amplitudes determined from any reference frame. In particular, this innovative approach allows calculations in an asymmetric frame, applying all momentum transfer to the initial-state or final-state nucleon, rather than the commonly used symmetric frame. Consequently, multiple momentum transfers can be achieved through contractions without the need for additional inversions, leading to a faster and more efficient computation of GPDs using lattice QCD. In Refs. [93, 94], we presented the x -dependent twist-2 GPDs for unpolarized quarks, specifically H and E , across multiple values of the momentum transfer t , along with their moments up to the fifth order. In Ref. [100], we extend the theoretical framework to the case of axial-vector GPDs. Building on this progress, in the present work, we extract the Mellin moments of the zero-skewness axial-vector GPD $\tilde{H}(x, 0, t)$ over a wide range of t , and we discuss the physical insights that these moments provide.

This work is organized as follows. In Sec. 2, we review the theoretical framework of computing the quasi axial-vector GPD on the lattice. In Sec. 3, we show the bare matrix elements of the axial-vector iso-vector and iso-scalar GPDs and discuss the renormalization. In Sec. 4, we extract the first few moments from the ratio-scheme renormalized matrix elements using the next-to-leading order (NLO) SDF formula. For the first time, we get

access up to the fifth moment of the axial-vector GPD $\tilde{H}(x, \xi, t)$ with reasonable signal and t dependence. In Sec. 5, we discuss the relation between the moments and the spin structure of the nucleon, including the quark helicity and OAM contributions to the nucleon spin as well as the quark spin-orbit correlations. We also explore the distribution of these quantities in the impact parameter plane. Finally, Sec. 6 contains our conclusions.

2 Axial-vector GPD on the lattice

2.1 The definition of axial-vector GPDs

The quark GPDs of nucleon are defined as the Fourier transform of the off-forward matrix elements

$$F^{[\Gamma]}(z^-, \Delta, P) = \langle p_f; \lambda' | O_\Gamma | p_i; \lambda \rangle, \quad (2.1)$$

where p_i and p_f represent the momenta of the initial-state and final-state nucleon, respectively, while λ and λ' denote the helicities of the nucleons. After performing the Fourier transform over z^- , the GPDs become functions of the average longitudinal momentum fraction x of the quarks and two additional kinematic variables, typically chosen as the skewness ξ and the momentum transfer squared t . Using $P = (p_i + p_f)/2$ and $\Delta = p_f - p_i$, they are defined as

$$\xi = -\frac{\Delta^+}{2P^+}, \quad t = \Delta^2. \quad (2.2)$$

The quark bilinear operator involved is defined as,

$$O_\Gamma = \bar{\psi}(-\frac{z^-}{2}) \Gamma \mathcal{W}(-\frac{z^-}{2}, \frac{z^-}{2}) \psi(\frac{z^-}{2}), \quad (2.3)$$

where the quark fields are separated along the light-cone and connected by a Wilson line to ensure gauge invariance,

$$\mathcal{W}(-\frac{z^-}{2}, \frac{z^-}{2}) = \mathcal{P} \exp\left(-ig \int_{-\frac{z^-}{2}}^{\frac{z^-}{2}} dy^- A^+(0^+, y^-, \vec{0}_\perp)\right). \quad (2.4)$$

In the light-cone gauge $A^+ = 0$, the Wilson line vanishes, allowing the operator O_Γ to be interpreted as a particle density operator. For example, setting $\Gamma = \gamma^+(1 + \gamma_5)/2$ and $\gamma^+(1 - \gamma_5)/2$ corresponds to the density of right-handed and left-handed quarks inside the hadron, respectively. When summed, they give $\Gamma = \gamma^+$, providing the total quark number density. Their difference ($\Gamma = \gamma^+\gamma_5$) yields the quark helicity density, a crucial quantity for understanding the spin structure of the hadron.

In this work, we study the axial-vector GPDs defined through $\Gamma = \gamma^+\gamma_5$. At the twist-2 level, there are two distinct axial-vector GPDs, \tilde{H} and \tilde{E} , defined through [8]

$$F^{[\gamma^+\gamma_5]}(z^-, \Delta, P) = \bar{u}(p_f, \lambda') \left[\gamma^+\gamma_5 \tilde{H}(z^-, \xi, t) + \frac{\Delta^+\gamma_5}{2m} \tilde{E}(z^-, \xi, t) \right] u(p_i, \lambda). \quad (2.5)$$

Since we are focusing on $\xi = 0$ case, the kinematic factor associated with \tilde{E} vanishes, implying that this GPD cannot be extracted from our lattice data. Here, we therefore concentrate on the GPD \tilde{H} . We note that \tilde{E} also enters at the twist-3 level, where it can be addressed even for $\xi = 0$ [95, 101].

2.2 The axial-vector quasi GPD $\tilde{\mathcal{H}}$

The light-cone GPDs can be accessed from lattice QCD through the quasi-GPD approach in the large momentum limit. However, unlike light-cone GPDs, which are frame-independent, quasi-GPDs are frame-dependent at finite momentum. Traditionally, a specific symmetric frame was chosen. However, this choice is computationally very expensive, requiring separate, full computations—including inversions and contractions on the lattice—for each value of t . To address this problem, we proposed constructing quasi-GPDs using Lorentz-invariant amplitudes derived from the decomposition of the matrix elements [90]. This method eliminates the frame dependence, allowing any computationally preferred frame to be used. It is important to note that this decomposition is not unique and depends on the choice of basis. However, any basis will result in the same number of independent amplitudes. For the axial current we adopted the following decomposition [100],

$$\begin{aligned}
F^{[\gamma^\mu\gamma_5]}(z, P, \Delta) &\equiv \langle p_f; \lambda' | \bar{\psi}(-\frac{z}{2}) \gamma^\mu \gamma_5 \mathcal{W}(-\frac{z}{2}, \frac{z}{2}) \psi(\frac{z}{2}) | p_i; \lambda \rangle \\
&= \bar{u}(p_f, \lambda') \left[\frac{i\epsilon^{\mu P z \Delta}}{m} \tilde{A}_1 + \gamma^\mu \gamma_5 \tilde{A}_2 + \gamma_5 \left(\frac{P^\mu}{m} \tilde{A}_3 + m z^\mu \tilde{A}_4 + \frac{\Delta^\mu}{m} \tilde{A}_5 \right) \right. \\
&\quad \left. + m \not{z} \gamma_5 \left(\frac{P^\mu}{m} \tilde{A}_6 + m z^\mu \tilde{A}_7 + \frac{\Delta^\mu}{m} \tilde{A}_8 \right) \right] u(p_i, \lambda), \tag{2.6}
\end{aligned}$$

where $\epsilon^{\mu P z \Delta} = \epsilon^{\mu\alpha\beta\gamma} P_\alpha z_\beta \Delta_\gamma$ and $\tilde{A}_i \equiv \tilde{A}_i(z \cdot P, z \cdot \Delta, \Delta^2, z^2)$ are Lorentz invariant amplitudes that depend on Lorentz scalars. The case of the light-cone axial-vector GPDs defined in Eq. (2.5) corresponds to $\mu = +$ and $z = (z^+, z^-, z_\perp) = (0, z^-, 0_\perp)$. Thus, the GPD \tilde{H} can be expressed as

$$\begin{aligned}
\tilde{H}(z \cdot P, z \cdot \Delta, \Delta^2) &= \tilde{A}_2 + (P^+ z^-) \tilde{A}_6 + (\Delta^+ z^-) \tilde{A}_8 \\
&= \tilde{A}_2 + (P \cdot z) \tilde{A}_6 + (\Delta \cdot z) \tilde{A}_8. \tag{2.7}
\end{aligned}$$

As mentioned earlier, light-cone GPDs cannot be directly simulated in Euclidean lattice QCD. In this work, we consider quasi-GPDs, which maintain the same form as Eq. (2.5) but are defined at equal time ($z^0 = 0$). In this approach, quarks are separated along the spatial direction $\mathbf{z} = (0, 0, z^3)$ with a large momentum $\mathbf{P} = (0, 0, P^3)$. Typically, $\gamma^\mu \gamma_5 = \gamma^3 \gamma_5$ is chosen to approach the light-cone limit, as it avoids operator mixing caused by explicit chiral symmetry breaking which affects $\gamma^0 \gamma_5$ [102, 103]. This means, we consider

$$F^{[\gamma^3\gamma_5]}(z, P, \Delta) = \bar{u}(p_f, \lambda') \left[\gamma^3 \gamma_5 \tilde{\mathcal{H}}_3(z, \xi, t) + \frac{\Delta^3 \gamma_5}{2m} \tilde{\mathcal{E}}_3(z, \xi, t) \right] u(p_i, \lambda). \tag{2.8}$$

According to Eq. (2.6), the axial-vector quasi GPDs can be expressed as

$$\begin{aligned}
\tilde{\mathcal{H}}_3(z, P, \Delta) &= \tilde{A}_2 - z^3 P^3 \tilde{A}_6 - m^2 (z^3)^2 \tilde{A}_7 - z^3 \Delta^3 \tilde{A}_8 \\
&= \tilde{A}_2 + (P \cdot z) \tilde{A}_6 + m^2 z^2 \tilde{A}_7 + (\Delta \cdot z) \tilde{A}_8. \tag{2.9}
\end{aligned}$$

Compared to Eq. (2.7), the Lorentz invariant amplitudes $\tilde{A}_i(z \cdot P, z \cdot \Delta, \Delta^2, z^2)$ in $\tilde{\mathcal{H}}_3$ implicitly depend on the finite $z^2 = -|\mathbf{z}|^2$, which is zero in the light-cone case. In addition,

$\tilde{\mathcal{H}}_3$ explicitly includes an additional contamination term $m^2 z^2 \tilde{A}_7$ due to the non-vanishing z^2 . In Refs. [90, 100], it was proposed to remove these explicit power corrections and construct Lorentz-invariant (LI) matrix elements, as in Eq. (2.7), through the Lorentz-invariant amplitudes \tilde{A}_i , which can be extracted from the linear combination of quasi-GPDs with different spin structures. As discussed in detail in Ref. [100], the LI axial-vector GPDs in Eq. (2.7) can be derived from the linear combination of $F^{[\gamma^\mu \gamma_5]}$ with $\mu = 0, 1, 2$, referred to as $\tilde{\mathcal{H}}$. We note that the only difference between the quasi GPD $\tilde{\mathcal{H}}$ and light-cone GPD \tilde{H} is the non-zero z^2 in \tilde{A}_i . Interestingly, it was found in Ref. [100] that the term $m^2 z^2 \tilde{A}_7$ is mostly consistent with zero, so that $\tilde{\mathcal{H}}_3$ and $\tilde{\mathcal{H}}$ are largely consistent within statistical errors. Therefore, we can focus on $\tilde{\mathcal{H}}_3$ in the following analysis without concerns about the contamination term $m^2 z^2 \tilde{A}_7$. Additionally, we repeat that $\tilde{\mathcal{H}}_3$ has the advantage of avoiding operator mixing due to explicit chiral symmetry breaking from lattice discretization [102, 103].

3 Bare matrix elements and renormalization

3.1 Lattice setup

The data used in this work has been analyzed in Ref. [100], to derive the x -dependent GPD in the LaMET framework. In this study, however, we focus on extracting the first few moments of GPDs using the SDF approach. The data were obtained from a gauge ensemble of $N_f = 2 + 1 + 1$ twisted-mass fermions with a clover term and Iwasaki-improved gluons [104]. The lattice size and spacing of the ensemble are $N_s \times N_t = 32^3 \times 64$ and $a = 0.0934$ fm, respectively, with quark masses corresponding to a pion mass of 260 MeV.

The quasi-GPD matrix elements are extracted from the three-point functions,

$$C_\mu^{\text{3pt}}(\Gamma_\kappa, p_f, p_i; t_s, \tau) = \sum_{\vec{y}, \vec{z}_0} e^{-i\vec{p}_f \cdot (\vec{y} - \vec{x})} e^{-i\vec{q} \cdot (\vec{x} - \vec{z}_0)} \Gamma_{\alpha\beta}^\kappa \langle N_\alpha^{(s)}(\vec{y}, t_s) \mathcal{O}_\mu(\vec{z}_0 + z\hat{z}, \tau) \bar{N}_\beta^{(s)}(\vec{x}, 0) \rangle, \quad (3.1)$$

where \vec{x} is the source position, $N^{(s)}$ is the standard nucleon source under momentum smearing [105] to improve the overlap with the proton ground state and suppress gauge noise. The quasi-GPD operator $\mathcal{O}_\mu = \bar{\psi}(z) \gamma^\mu \gamma_5 \mathcal{W}(z, 0) \psi(0)$ has quark fields separated along the z_3 direction. Both the iso-vector ($u-d$) and iso-scalar ($u+d$) flavor combinations were computed with the disconnected diagrams ignored for the iso-scalar case. In Ref. [106], it was found that, on the same ensemble as this work, the disconnected contributions for the forward limit are tiny; they would be further suppressed in off-forward kinematics. The unpolarized and polarized parity projectors Γ_0 and Γ_κ are defined as,

$$\Gamma_0 = \frac{1}{4} (1 + \gamma_0), \quad (3.2)$$

$$\Gamma_\kappa = \frac{1}{4} (1 + \gamma_0) i\gamma_5 \gamma_\kappa, \quad \kappa = 1, 2, 3. \quad (3.3)$$

frame	P_3 [GeV]	Δ [$\frac{2\pi}{L}$]	$-t$ [GeV ²]	ξ	N_{ME}	N_{confs}	N_{src}	N_{tot}
N/A	± 1.25	(0,0,0)	0	0	2	329	16	10528
symm	± 0.83	($\pm 2, 0, 0$), ($0, \pm 2, 0$)	0.69	0	8	67	8	4288
symm	± 1.25	($\pm 2, 0, 0$), ($0, \pm 2, 0$)	0.69	0	8	249	8	15936
symm	± 1.67	($\pm 2, 0, 0$), ($0, \pm 2, 0$)	0.69	0	8	294	32	75264
symm	± 1.25	($\pm 2, \pm 2, 0$)	1.38	0	16	224	8	28672
symm	± 1.25	($\pm 4, 0, 0$), ($0, \pm 4, 0$)	2.77	0	8	329	32	84224
asymm	± 1.25	($\pm 1, 0, 0$), ($0, \pm 1, 0$)	0.17	0	8	269	8	17216
asymm	± 1.25	($\pm 1, \pm 1, 0$)	0.34	0	16	195	8	24960
asymm	± 1.25	($\pm 2, 0, 0$), ($0, \pm 2, 0$)	0.65	0	8	269	8	17216
asymm	± 1.25	($\pm 1, \pm 2, 0$), ($\pm 2, \pm 1, 0$)	0.81	0	16	195	8	24960
asymm	± 1.25	($\pm 2, \pm 2, 0$)	1.24	0	16	195	8	24960
asymm	± 1.25	($\pm 3, 0, 0$), ($0, \pm 3, 0$)	1.38	0	8	269	8	17216
asymm	± 1.25	($\pm 1, \pm 3, 0$), ($\pm 3, \pm 1, 0$)	1.52	0	16	195	8	24960
asymm	± 1.25	($\pm 4, 0, 0$), ($0, \pm 4, 0$)	2.29	0	8	269	8	17216

Table 1. Statistics for the symmetric and asymmetric frame matrix elements are shown. The momentum unit $2\pi/L$ is 0.417 GeV. N_{ME} , N_{confs} , N_{src} and N_{total} are the number of matrix elements, configurations, source positions per configuration and total statistics, respectively.

To derive the ground-state matrix elements, we also computed the two-point functions for the energy spectrum and overlap amplitudes $\langle \Omega | N^{(s)} | N \rangle$, which are given by,

$$C^{2\text{pt}}(\Gamma_0, p; t_s) = \sum_{\vec{y}} e^{-i\vec{p} \cdot (\vec{y} - \vec{x})} \Gamma_{\alpha\beta}^0 \langle N_{\alpha}^{(s)}(\vec{y}, t_s) \bar{N}_{\beta}^{(s')}(\vec{x}, 0) \rangle. \quad (3.4)$$

Since the two- and three-point functions are highly correlated, we construct the ratio,

$$R_{\kappa}^{\mu}(\Gamma_{\kappa}, p_f, p_i; t_s, \tau) = \frac{C_{\mu}^{3\text{pt}}(\Gamma_{\kappa}, p_f, p_i; t_s, \tau)}{C^{2\text{pt}}(\Gamma_0, p_f; t_s)} \sqrt{\frac{C^{2\text{pt}}(\Gamma_0, p_i, t_s - \tau) C^{2\text{pt}}(\Gamma_0, p_f, \tau) C^{2\text{pt}}(\Gamma_0, p_f, t_s)}{C^{2\text{pt}}(\Gamma_0, p_f, t_s - \tau) C^{2\text{pt}}(\Gamma_0, p_i, \tau) C^{2\text{pt}}(\Gamma_0, p_i, t_s)}}, \quad (3.5)$$

which, in the $t_s \rightarrow \infty$ limit, corresponds to the bare matrix elements of proton ground state $\lim_{t_s \rightarrow \infty} R_{\kappa}^{\mu} = \Pi_{\mu}(\Gamma_{\kappa})$. To keep the statistical noise under control, we use a source-sink separation of $t_s = 10a = 0.93$ fm and perform a plateau fit with respect to the time insertion τ in a region of convergence. More details can be found in Ref. [100]. A more thorough study of excited state contamination will be left for future work that targets precision control.

In Table 1, we show the momenta $\vec{P} = (0, 0, P_3)$ and $\vec{\Delta}$ as well as the statistics used in this work. For the symmetric frame, the momentum components are defined as,

$$\vec{p}_f^s = \vec{P} + \frac{\vec{\Delta}}{2} = \left(+\frac{\Delta_1}{2}, +\frac{\Delta_2}{2}, P_3 \right), \quad \vec{p}_i^s = \vec{P} - \frac{\vec{\Delta}}{2} = \left(-\frac{\Delta_1}{2}, -\frac{\Delta_2}{2}, P_3 \right), \quad (3.6)$$

In contrast, for the asymmetric frame, where all momentum transfer is assigned to the initial state, we have,

$$\vec{p}_f^a = \vec{P} = (0, 0, P_3), \quad \vec{p}_i^a = \vec{P} - \vec{\Delta} = (-\Delta_1, -\Delta_2, P_3). \quad (3.7)$$

While \vec{P} and $\vec{\Delta}$ are the same for both frames, they lead to slightly different values of $-t$ due to the different distribution of the momentum transfer, that is

$$-t^s = \vec{\Delta}^2, \quad -t^a = \vec{\Delta}^2 - (E(p') - E(p))^2. \quad (3.8)$$

This work focuses on zero skewness, namely $\Delta_3 = 0$. As already mentioned above, this does not give us access to the GPD \tilde{E} . Most of the hadron momentum P is fixed at 1.25 GeV throughout the calculation. We combine all data contributing to the same value of momentum transfer $t = -\Delta^2$ with definite symmetry with respect to $P_3 \rightarrow -P_3$, $z_3 \rightarrow -z_3$, and $\vec{\Delta} \rightarrow -\vec{\Delta}$ [100].

3.2 Bare matrix elements and renormalization

The bare matrix elements for the quasi axial-vector GPD $\tilde{\mathcal{H}}_3$ are shown in Fig. 1, where a clear signal is observed across a wide range of momentum transfers $-t$. The bare matrix elements need to be renormalized. At $z = 0$ and $\Delta = 0$, the iso-vector matrix element $\tilde{\mathcal{H}}_3^B$ gives the bare iso-vector axial charge of the nucleon, g_A^B , which needs to be renormalized by the constant Z_A . The Z_A for this ensemble has been determined as 0.7442 [100], leading to a derived $g_A = 1.164(13)$ using $\tilde{\mathcal{H}}_3^{B,u-d}(0, 0, 0)$. This value is consistent with results in Ref. [107] with similar quark masses. For the case of non-zero z_3 , it has been shown that the non-local operator O_{Γ} can be multiplicatively renormalized [108–110],

$$O_{\Gamma}(z) = Z_O e^{-\delta m|z|} O_{\Gamma}^R(z), \quad (3.9)$$

where Z_O accounts for logarithmic divergences, and the exponential factor $e^{-\delta m|z|}$ removes the linear divergence stemming from the self-energy of the spatial Wilson link. Since this renormalization is independent of the hadron state and quark flavor, one can construct an appropriate ratio to eliminate UV divergences and obtain renormalization group invariant quantities [71, 72, 111, 112],

$$\mathcal{M}(z_3, P_3, \Delta) = \frac{\tilde{\mathcal{H}}_3^B(z_3, P_3, \Delta; a)}{\tilde{\mathcal{H}}_3^B(z_3, 0, 0; a)} \cdot g_A = \frac{\tilde{\mathcal{H}}_3^R(z_3, P_3, \Delta; \mu)}{\tilde{\mathcal{H}}_3^R(z_3, 0, 0; \mu)} \cdot g_A. \quad (3.10)$$

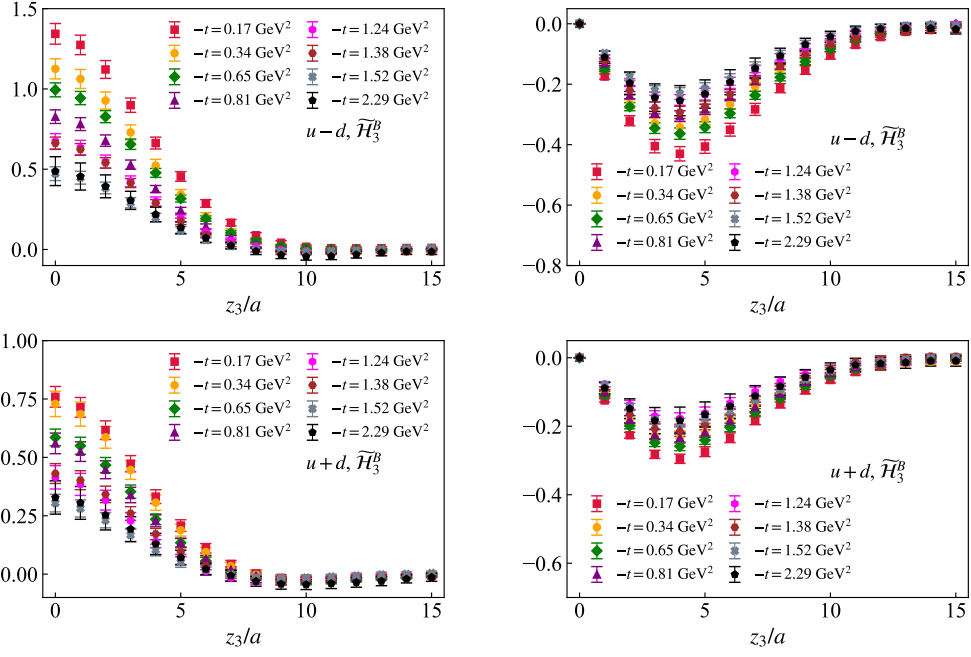


Figure 1. Bare matrix elements are shown as a function of z_3/a for different values of t . The iso-vector ($u - d$) and iso-scalar ($u + d$) case are shown in the upper and lower panels, respectively. The left panels show the real part while the right panels show the imaginary part.

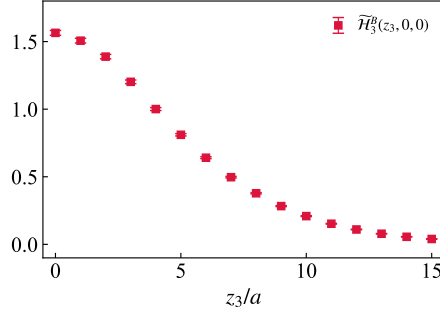


Figure 2. Zero momentum iso-vector axial-vector quasi-PDF matrix elements.

We multiply $g_A = Z_A \tilde{\mathcal{H}}_3^{B,u-d}(0, 0, 0; a)$ to normalize the iso-vector $\mathcal{M}(0, 0, 0)$ to g_A . This choice of convention will be explained in the next section. In this ratio, the matrix elements in the denominator correspond to axial-vector quasi-PDF matrix elements with zero momentum $P = 0$ and zero momentum transfer $\Delta = 0$. Since UV divergences are independent of the light quark flavors, we consistently use the iso-vector $\tilde{\mathcal{H}}_3^{B,u-d}(z_3, 0, 0)$ as the denominator in this work, which are shown in Fig. 2. Both the iso-vector and iso-scalar $\tilde{\mathcal{H}}_3^B(z, P, \Delta)$ are used in the numerator. It should be noted again that the disconnected diagrams were omitted for the iso-scalar case in this study.

In Fig. 3, the real and imaginary parts of the ratio scheme renormalized matrix elements are presented as a function of z_3 for both the iso-vector and iso-scalar cases. As one can see,

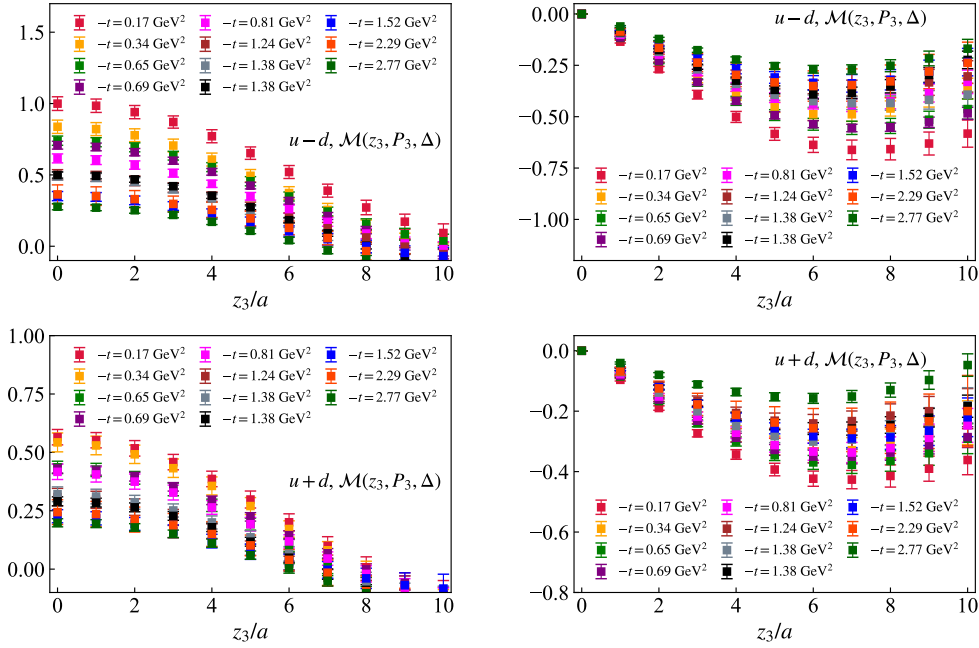


Figure 3. Ratio scheme renormalized matrix elements are shown as a function of z_3/a . The iso-vector ($u - d$) and iso-scalar ($u + d$) case are shown in the upper and lower panels, respectively. The left panels show the real part while the right panels show the imaginary part.

the expected $-t$ dependence is clearly visible, with the magnitude of the matrix elements decreasing monotonically as $-t$ increases.

4 Mellin moments from short distance factorization

4.1 Short distance factorization

In the short-distance limit, the renormalized matrix elements can be expanded in terms of the Mellin moments using the operator product expansion (OPE). For the zero-skewness quasi-GPD under consideration, the OPE structure mirrors that of the quasi-PDF case, without any mixing between moments. In the $\overline{\text{MS}}$ scheme, the short-distance factorization (SDF) of the iso-vector quasi-GPD matrix elements can be expressed as,

$$\tilde{\mathcal{H}}_3^R(z_3, P_3, \Delta; \mu) = \sum_{n=0}^{\infty} C_n^{\overline{\text{MS}}}(\mu^2 z^2) \frac{(-iz_3 P_3)^n}{n!} \tilde{A}_{n+1,0}(t; \mu) + \mathcal{O}(\Lambda_{\text{QCD}}^2 z^2), \quad (4.1)$$

where the

$$\tilde{A}_{n+1,0}(t; \mu) = \int_{-1}^1 dx x^n \tilde{H}(x, \xi = 0, t; \mu) \quad (4.2)$$

represent the Mellin moments of the axial-vector GPD at zero skewness. It's worth to mention that the first moment $\tilde{A}_{1,0}(t; \mu)$ is the nucleon axial form factor corresponding to the local matrix elements $\tilde{\mathcal{H}}_3^R(0, P_3, \Delta; \mu)$. $C_n(\mu^2 z^2)$ are the Wilson coefficients. At

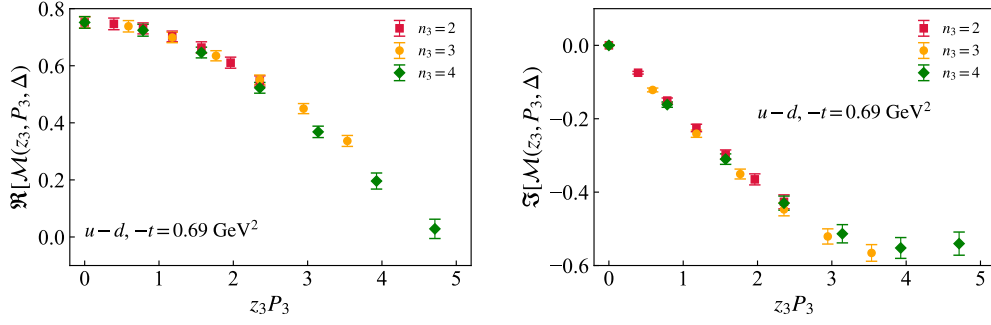


Figure 4. The ratio scheme renormalized iso-vector matrix elements for $-t = 0.69 \text{ GeV}^2$ are shown as a function of $z_3 P_3$ for three different values of P_3 . The real part (left panel) and imaginary part (right panel) are both shown.

leading order (LO), $C_n(\mu^2 z^2) = 1$, making Eq. (4.1) a simple polynomial function of the so-called Ioffe time $\zeta = z_3 P_3$. Beyond LO, the perturbative corrections account for the scale evolution from the physical scale $\sim 1/z_3$ to the factorization scale μ , which at NLO are given by [113],

$$C_n^{\overline{\text{MS}}}(\mu^2 z^2) = 1 + \frac{\alpha_s C_F}{2\pi} \left[\left(\frac{3+2n}{2+3n+n^2} + 2H_n \right) L_z + \frac{7+2n}{2+3n+n^2} + 2(1-H_n)H_n - 2H_n^{(2)} \right], \quad (4.3)$$

with $L_z = \ln(\mu^2 z^2 e^{2\gamma_E}/4)$ and the Harmonic numbers $H_n = \sum_{i=1}^n 1/i$ and $H_n^{(2)} = \sum_{i=1}^n 1/i^2$. This SDF formula can be inserted into Eq. (3.10), establishing a relationship between the renormalized matrix elements and the moments of the GPDs,

$$\begin{aligned} \mathcal{M}(z_3, P_3, \Delta) &= \frac{\sum_{n=0}^{\infty} C_n^{\overline{\text{MS}}}(\mu^2 z^2) \frac{(-iz_3 P_3)^n}{n!} \tilde{A}_{n+1,0}(t; \mu) + \mathcal{O}(\Lambda_{\text{QCD}}^2 z^2)}{C_0^{\overline{\text{MS}}}(\mu^2 z^2) \tilde{A}_{1,0}^{u-d}(0; \mu) + \mathcal{O}(\Lambda_{\text{QCD}}^2 z^2)} \cdot g_A \\ &= \sum_{n=0}^{\infty} \frac{C_n^{\overline{\text{MS}}}(\mu^2 z^2)}{C_0^{\overline{\text{MS}}}(\mu^2 z^2)} \frac{(-iz_3 P_3)^n}{n!} \tilde{A}_{n+1,0}(t) + \mathcal{O}(\Lambda_{\text{QCD}}^2 z^2). \end{aligned} \quad (4.4)$$

We note again, the denominator in Eq. (3.10) is solely the iso-vector matrix element while the numerator can be either iso-vector and iso-scalar. As a result, $\tilde{A}_{1,0}^{u-d}(0; \mu) = g_A$ cancels out in the first line of the formula. This explains our choice of ratio defined in Eq. (3.10). From this expression, the even and odd moments of the axial-vector GPD can be extracted from the real and imaginary parts of $\mathcal{M}(z_3, P_3, \Delta)$, respectively. Notably, it is crucial to keep z^2 small to avoid large power corrections. At present, lattice calculations are limited to finite values of P_3 , which in our case are listed in Table 1, allowing the extraction of only the first few moments within a limited kinematic range of $z_3 P_3$.

4.2 Moments from fixed z^2

For $-t = 0.69 \text{ GeV}^2$, we have three different momenta with $n_3 = 2, 3, 4$ corresponding to 0.83, 1.25, 1.67 GeV, respectively. This allows us to extract moments from each single z_3

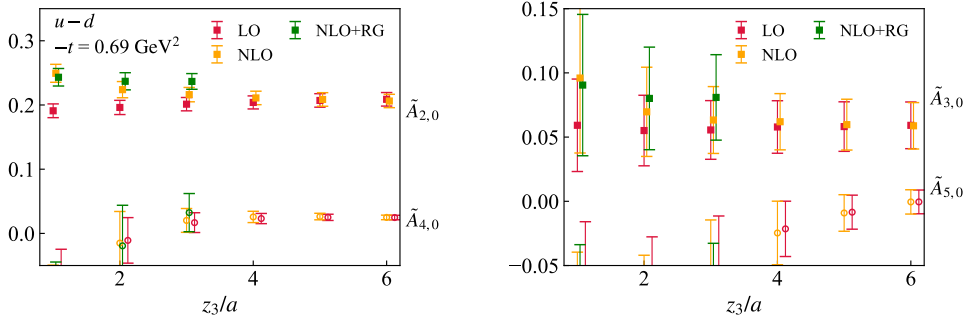


Figure 5. The iso-vector moments at momentum transfer $-t = 0.69 \text{ GeV}^2$, derived from fits of P_3 dependence, are shown as a function of z_3 .

by fitting the P_3 dependence. In this section, we consider the matching formula at LO, NLO, as well as renormalization group improved NLO (NLO+RG) [97, 114–116] accuracy. If the perturbative matching can describe the evolution well, the moments for a given factorization scale μ should be independent for different values of z_3 .

In Fig. 4, we present the ratio scheme renormalized matrix elements for the iso-vector case as a function of $z_3 P_3$. One can see from the plots that the dependence of the results on P_3 is very weak. This is expected because, when the perturbative evolution encoded in $C_n^{\overline{\text{MS}}}(\mu^2 z^2)$ and the power corrections are both small within the short z_3 range ($z_3 \lesssim 3a$) and cancel to a good degree in the ratio, the renormalized matrix element should depend solely on $z_3 P_3$ within the current statistical error [94, 112]. To extract the moments according to Eq. (4.4), we minimize,

$$\chi_{z_3}^2 = \sum_{P_3} \left(\frac{(\text{Re}[\mathcal{M}^{\text{data}}(z_3, P_3, \Delta)] - \text{Re}[\mathcal{M}^{\text{SDF}}(z_3, P_3, \Delta)])^2}{\sigma_{\text{Re}}^2} + \frac{(\text{Im}[\mathcal{M}^{\text{data}}(z_3, P_3, \Delta)] - \text{Im}[\mathcal{M}^{\text{SDF}}(z_3, P_3, \Delta)])^2}{\sigma_{\text{Im}}^2} \right), \quad (4.5)$$

where σ_{Re} and σ_{Im} represent the errors in the real and imaginary parts of $\mathcal{M}^{\text{data}}(z_3, P_3, \Delta)$, respectively.

The moments obtained from the fits are shown in Fig. 5 as a function of z_3 . The results are evaluated at $\mu = 2 \text{ GeV}$. We omit the discussion of the axial form factor $\tilde{A}_{1,0}$ here, as it is determined from local matrix elements, requiring neither the SDF nor dependence on z_3 . For the first two non-trivial moments, $\tilde{A}_{2,0}$ and $\tilde{A}_{3,0}$, a reasonable signal emerges starting from $z_3 = a$. However, for the higher moments a clear signal can only be obtained for larger values of z_3 . As one can see, $\tilde{A}_{2,0}$ exhibits a mild z_3 dependence for $z_3 < 4a$ when LO and NLO Wilson coefficients are used. This mild dependence is due to a combination of discretization effects, which could be especially large for $z_3 = a$, and missing higher-order terms in the Wilson coefficients. The results that use NLO Wilson coefficients with RG improved coefficients are only shown for z_3 up to $3a$, as for larger z_3 values the scale is too low to evaluate the strong coupling constant α_s . In that range, the NLO results and NLO results with RG resummation are consistent.

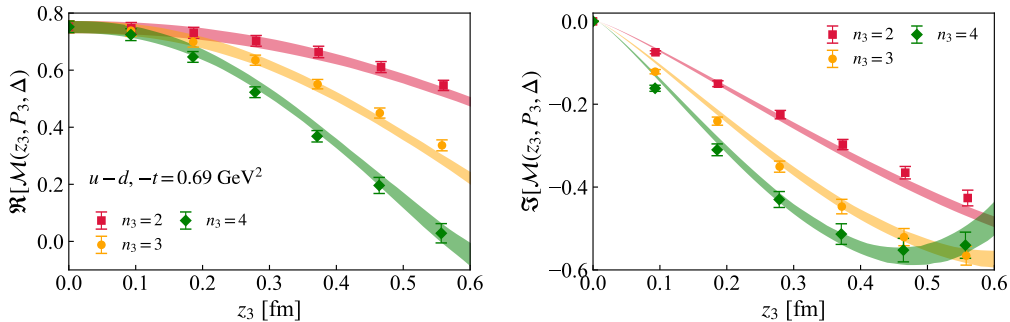


Figure 6. The ratio scheme renormalized iso-vector matrix elements for the case with momentum transfer $-t = 0.69\text{GeV}^2$ are shown as a function of z_3 for three different values of P_3 . The real part (left panel) and imaginary part (right panel) are both shown. The bands are reconstructed from the fit with $z_3 \in [2a, 6a]$ including the NLO matching kernels.

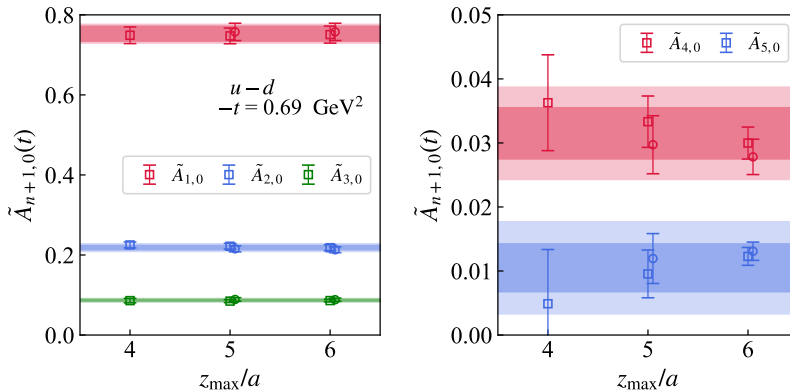


Figure 7. The moments obtained from combined fit using matrix element with $z_3 \in [z_{\min}, z_{\max}]$ and $n_3 = 2, 3, 4$ are shown as a function of z_{\max} . The squared symbols are results from $z_{\min} = 2a$ while the circled symbols are from $z_{\min} = 3a$.

4.3 Moments from combined fits

Since the factorization formula with NLO coefficient can describe the lattice data reasonably well, in this section we perform combined fits of matrix elements with different n_3 in a range of $z_3 \in [z_{\min}, z_{\max}]$. Specifically, we minimize the $\chi^2 = \sum_{z_3} \chi_{z_3}^2$. The combined fits are more stable than the fits for fixed z_3 values. To avoid the most serious discretization effects, we skip the point $z_3 = a$. We vary $z_{\min} \in [2a, 3a]$ to estimate the discretization effects and $z_{\max} \in [z_{\min} + 2a, 6a]$ to estimate the higher-twist effects. The resulting fit yields a reasonable $\chi^2/\text{d.o.f.}$, and the bands reconstructed from the fit accurately describe the renormalized matrix elements, as shown in Fig. 6.

The extracted moments are shown in Fig. 7. The squared symbols represent results from $z_{\min} = 2a$, while the circled symbols correspond to $z_{\min} = 3a$. As illustrated, the results from the two z_{\min} values overlap, indicating that discretization effects are minimal compared to the statistical errors. Regarding the z_{\max} dependence, it appears negligible within the errors, particularly for the lower moments. However, higher moments require

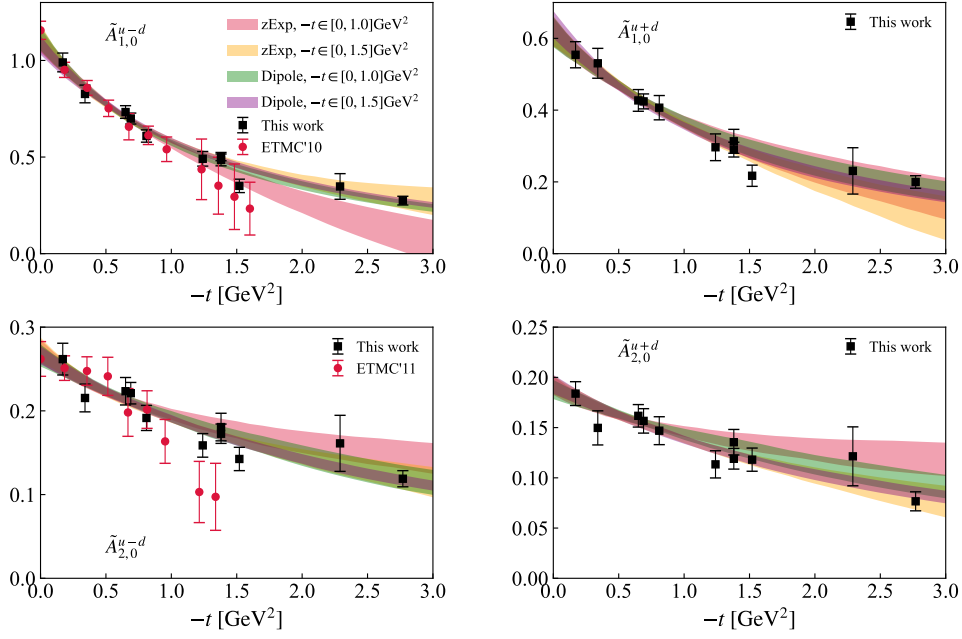


Figure 8. The first and second Mellin moments $\tilde{A}_{1,0}$ and $\tilde{A}_{2,0}$ of the axial-vector GPDs are shown. The left panels are the iso-vector results while the right panels are the iso-scalar results. The bands are results from z -expansion (zExp) and dipole methods by fitting data in the ranges $-t \in [0, 1.0]$ GeV² and $-t \in [0, 1.5]$ GeV². For comparison, we also show results derived from traditional local operator methods with the same pion mass for the iso-vector case (ETMC) [107, 118].

larger z_{\max} values to stabilize the fit.

For the final estimates, we average the results obtained from different choices of z_{\min} and z_{\max} , with their deviations treated as systematic errors, as we did in Refs. [94, 112]. These results are depicted as bands in Fig. 7, with the darker and lighter bands representing statistical and systematic errors, respectively, covering the relevant data points.

We extended this analysis to all other values of the momentum transfer listed in Table 1, covering both iso-vector and iso-scalar cases. For the latter, we neglected the mixing with the gluon distribution starting from $\mathcal{O}(\alpha_s)$ [117]. In Fig. 8, we summarize our determination of first two moments, $\tilde{A}_{1,0}$ and $\tilde{A}_{2,0}$, as functions of $-t$. For comparison, we show results obtained from traditional local operator methods with a similar lattice setup and pion mass for the iso-vector case (ETMC) [107, 118]. It is encouraging that our results align with the previous ETMC findings, suggesting that our extraction of the moments from non-local operators is effective. Notably, we are also able to extract higher moments up to $\tilde{A}_{5,0}$ for the first time, as shown in Fig. 9. As one can see from the figure, we obtain a reasonable signal, and the $-t$ dependence of the results follows the general expectations. We note that we apply the z -expansion and a dipole fit, and for each we compare the parametrization of the t dependence using data up to 1.0 GeV² and 1.5 GeV². In most cases, the dipole fit and the z -expansion are in agreement. However, a difference is found between $-t_{\max} = 1.0$ GeV² and $-t_{\max} = 1.5$ GeV². More details are given in Sec.5.1.

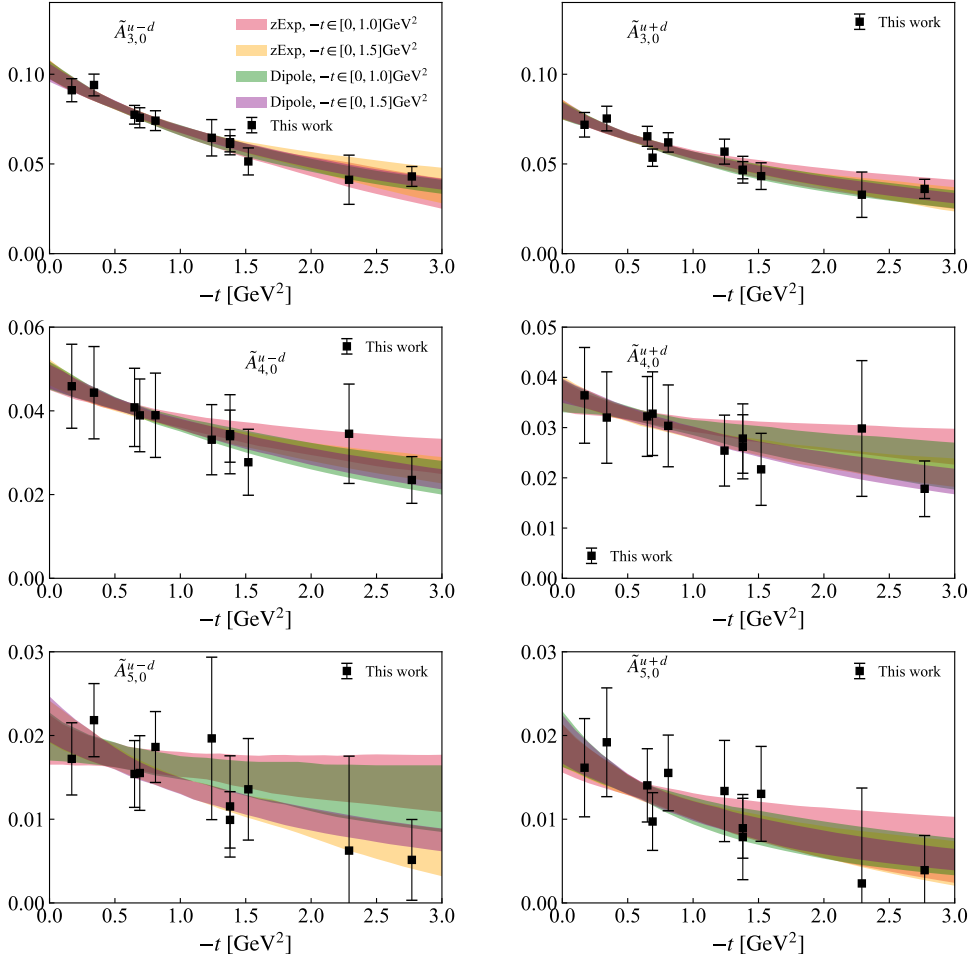


Figure 9. The Mellin moments $\tilde{A}_{3,0}$, $\tilde{A}_{4,0}$ and $\tilde{A}_{5,0}$ of the axial-vector GPDs are shown. The left panels are the iso-vector results while the right panels are the iso-scalar results. The bands are results from z -expansion (zExp) and dipole methods by fitting data in the ranges $-t \in [0, 1.0]$ GeV² and $-t \in [0, 1.5]$ GeV².

5 Insights into nucleon spin dynamics from axial vector GPD

GPDs offer crucial insights into the spin structure of the nucleon. For instance, in a longitudinally polarized nucleon, the contributions to the nucleon spin \mathbf{S}_z^N from quark helicity, orbital angular momentum (OAM), and total spin are represented by $\langle \mathbf{S}_z^q \mathbf{S}_z^N \rangle$, $\langle \mathbf{L}_z^q \mathbf{S}_z^N \rangle$ and $\langle \mathbf{J}_z^q \mathbf{S}_z^N \rangle$, respectively, where $\langle \dots \rangle$ denotes the appropriate average. At $-t = 0$, the first moment of the axial-vector GPD \tilde{H} is directly connected to the quark helicity contribution, expressed as,

$$S_z^q = \frac{1}{2} \int_{-1}^1 dx \tilde{H}^q(x, 0, 0) = \frac{1}{2} \tilde{A}_{1,0}^q(0). \quad (5.1)$$

According to Ji's spin sum rule [2], the contribution of the total angular momentum of quarks J_z^q to the nucleon spin can be derived from the second moments of unpolarized

quark GPDs,

$$J_z^q = \frac{1}{2}(A_{2,0}^q(0) + B_{2,0}^q(0)), \quad (5.2)$$

where $A_{2,0}^q(0) = \int_{-1}^1 dx x H^q(x, \xi = 0, t = 0)$ and $B_{2,0}^q(0) = \int_{-1}^1 dx x E^q(x, \xi = 0, t = 0)$. We have determined J_z^q using the same lattice setup and framework in Ref. [94]. This allows us to determine the quark OAM contribution through,

$$L_z^q = J_z^q - S_z^q = \frac{1}{2}(A_{2,0}^q(0) + B_{2,0}^q(0)) - \frac{1}{2}\tilde{A}_{1,0}^q(0). \quad (5.3)$$

The quark spin-orbit correlation $\langle \mathbf{S}_z^q \mathbf{L}_z^q \rangle$ within the nucleon is another crucial aspect that can be probed through GPDs. This correlation describes how a quark's spin orientation is correlated to its orbital motion, offering deeper insights into the internal dynamics of hadrons. The spin-orbit correlation C_z^q can be derived as follows [16–18]¹,

$$\begin{aligned} C_z^q &= \frac{1}{2} \int_{-1}^1 dx x \tilde{H}^q(x, 0, 0) - \frac{1}{2} \left[\int_{-1}^1 dx H^q(x, 0, 0) - \frac{m_q}{2m_N} \int_{-1}^1 dx (E_T^q(x, 0, 0) + 2\tilde{H}_T^q(x, 0, 0)) \right] \\ &\approx \frac{1}{2} \int_{-1}^1 dx x \tilde{H}^q(x, 0, 0) - \frac{1}{2} \int_{-1}^1 dx H^q(x, 0, 0) \\ &= \frac{1}{2}(\tilde{A}_{2,0}^q(0) - A_{1,0}^q(0)), \end{aligned} \quad (5.4)$$

where we have ignored the term suppressed by the light quark mass. To determine C_z^q , one needs additional input from the first moment of the unpolarized quark GPD, $A_{1,0}^q(0) = \int_{-1}^1 dx H^q(x, \xi = 0, t = 0)$, giving the total quark number inside the nucleon.

In this section, we will discuss the quark helicity S_z^q , OAM L_z^q and spin-orbit correlation C_z^q derived from our GPD moments. With the broad range of $-t$ values available, we can also perform a Fourier transform and explore their distribution in impact parameter space.

5.1 Quark helicity, OAM, and spin-orbit correlations in nucleons

In Sec. 4.3, we have extracted the Mellin moments of axial-vector GPD $\tilde{H}(x, \xi = 0, -t)$ up to the fifth order. With multiple values of $-t$ ranging from 0.17 to 2.77 GeV², we can parameterize the $-t$ dependence and extrapolate to $-t \rightarrow 0$. One commonly used model in fitting nucleon form factors and moments is the dipole model,

$$\tilde{A}_{n,0}(-t) = \frac{\tilde{A}_{n,0}(0)}{(1 - \frac{t}{M^2})^2}, \quad (5.5)$$

where $\tilde{A}_{n,0}(0)$ and M are fit parameters. Empirically, this model has been successful in fitting form factors from experiments and lattice QCD at low $-t$. However, when the data

¹The quark spin-orbit correlation was first introduced using Wigner phase space distributions [119]; see also Ref. [120]. It depends on the path chosen for the Wilson line in the definition of the Wigner functions. The definition we are using here corresponds to a straight Wilson line connecting the quark fields of the corresponding bi-local operator. Related work can also be found in [121–123] and references therein.

span a wide range of $-t$, a more flexible parameterization is often preferred, such as the z -expansion series [124],

$$\tilde{A}_{n,0}(-t) = \sum_{k=0}^{k_{\max}} a_k z(t)^k, \quad (5.6)$$

with,

$$z(t) = \frac{\sqrt{t_{\text{cut}} - t} - \sqrt{t_{\text{cut}} - t_0}}{\sqrt{t_{\text{cut}} - t} + \sqrt{t_{\text{cut}} - t_0}} \quad (5.7)$$

where t_0 is selected to minimize the span of $z(t)$ over the given range of t , thereby optimizing the convergence of the series expansion. In this work, we apply $t_0 = t_{\text{cut}}(1 - \sqrt{1 - t_{\max}/t_{\text{cut}}})$ with t_{cut} set to be the three-pion kinematic threshold $(3m_\pi)^2$. To maintain a reasonable $\chi^2/\text{d.o.f.}$ and avoid overfitting, we truncate the series at $k_{\max} = 2$ in this work. To stabilize the fit, we imposed a Gaussian prior to the $|a_k/a_0|$ with a central value of 0 and width $|a_k/a_0|_{\max} = 5$.

To estimate the model bias, we vary the range of $-t$ included in the fit, specifically $-t \in [0, 1.0] \text{ GeV}^2$ and $-t \in [0, 1.5] \text{ GeV}^2$. Interestingly, the results from the dipole model not only go through the data point included in the fit but also can describe the data points at extended region up to 3 GeV^2 . In contrast, the z -expansion model, although flexible, sometimes fails to describe data points at higher $-t$ values, as it is a series expansion that can become unstable when extrapolated too far. For our final estimates, we average the results from different model choices and $-t$ ranges, taking their deviations as systematic errors, as done in previous studies [94, 112]. Our estimates of $\tilde{A}_{n+1,0}$ at $-t = 0$ are summarized in Table 2 for both the iso-vector and iso-scalar cases. The statistical and systematic uncertainties, shown in the first and second round brackets, respectively, are estimated based on the mean and deviation of results across various model choices and $-t$ ranges, following the approach used in previous studies [94, 112]. Our determination of the first two moments for the iso-vector case agrees with results from traditional local operators with a similar lattice setup and pion mass from ETMC [107, 118], where $\tilde{A}_{1,0}^{u-d} = 1.156(47)$ and $\tilde{A}_{2,0}^{u-d} = 0.262(21)$. We repeat that for the iso-scalar moments we omitted disconnected diagrams, which were found to be small on this ensemble [106], and the mixing with gluons in the perturbative matching, which starts at $\mathcal{O}(\alpha_s)$ [117].

The quark helicity can be derived from the first moment according to Eq. (5.1), yielding,

$$S_z^{u-d} = 0.555(29)(9), \quad S_z^{u+d} = 0.313(19)(6). \quad (5.8)$$

Our findings indicate that the light quark ($u + d$) helicity contribute significantly to the nucleon spin, consistent with results from previous lattice calculations (see, e.g., a recent review in Ref. [125]). In Ref. [94], using the same lattice setup and methodology, we determined the total quark contribution to the nucleon spin as $J_z^{u-d} = 0.281(21)(11)$ and $J_z^{u+d} = 0.296(22)(33)$. Consequently, we infer the quark orbital angular momentum (OAM) as,

$$L_z^{u-d} = -0.260(34)(19), \quad L_z^{u+d} = -0.010(37)(8). \quad (5.9)$$

$\tilde{A}_{1,0}^{u-d}$	1.110(57)(19)	$\tilde{A}_{1,0}^{u+d}$	0.625(38)(12)
$\tilde{A}_{2,0}^{u-d}$	0.270(12)(05)	$\tilde{A}_{2,0}^{u+d}$	0.191(9)(3)
$\tilde{A}_{3,0}^{u-d}$	0.102(5)(1)	$\tilde{A}_{3,0}^{u+d}$	0.080(5)(1)
$\tilde{A}_{4,0}^{u-d}$	0.049(3)(1)	$\tilde{A}_{4,0}^{u+d}$	0.037(3)(1)
$\tilde{A}_{5,0}^{u-d}$	0.021(3)(1)	$\tilde{A}_{5,0}^{u+d}$	0.019(3)(1)

Table 2. The Mellin moments of the axial-vector GPDs, \tilde{H} , extrapolated to $-t = 0$ are presented. The statistical and systematic uncertainties, shown in the first and second round brackets, respectively, are estimated based on the mean and deviation of results across various model choices and $-t$ ranges, following the approach used in previous studies [94, 112].

Interestingly, this result suggests that the light quark ($u + d$) OAM is very small [125]. However, this does not imply that the OAM of individual quarks are negligible, as the finite value of L_z^{u-d} indicates. Instead, the small total OAM for light quarks are likely due to the opposing signs of the OAM contributions from different quark flavors, leading to a cancellation effect.

Finally, we estimate the quark spin-orbit correlation using Eq. (5.4), combining $\tilde{A}_{2,0}$ from this work with $A_{1,0}$ from Ref. [94], which gives,

$$C_z^{u-d} = -0.356(20)(5), \quad C_z^{u+d} = -1.325(39)(14). \quad (5.10)$$

These results are in close agreement with previous findings in Refs. [16, 18]. Additionally, it is observed that the iso-vector spin-orbit correlation is significantly smaller than the iso-scalar one, consistent with predictions from the large N_c limit [126], which suggests that $C_z^{u-d} = \mathcal{O}(N_c^0)$ and $C_z^{u+d} = \mathcal{O}(N_c^1)$.

We note that, although these outcomes are encouraging, it is crucial to address systematic uncertainties arising from unphysical quark masses, disconnected diagrams, lattice discretization errors, and excited state contaminations in future works to achieve higher precision.

5.2 Impact-parameter-space interpretation

In addition to the spin decomposition discussed above, the GPDs also provide crucial insights into the three-dimensional structure of the nucleon. By performing a Fourier transform (FT) over the momentum transfer $-t$, we can derive parton distributions in the impact-parameter space. For instance, the quark helicity distribution in this space is given by,

$$\tilde{q}(x, \mathbf{b}_\perp) = \int \frac{d^2 \Delta_\perp}{(2\pi)^2} \tilde{H}(x, \xi = 0, \Delta_\perp^2) e^{i\mathbf{b}_\perp \cdot \Delta_\perp}, \quad (5.11)$$

where $-t = \Delta_\perp^2$. Its moments $\int_{-1}^1 dx x^n \tilde{q}(x, \mathbf{b}_\perp)$, which are the FT of the $\tilde{A}_{n+1,0}(-t)$, are averaged distributions with weight x^n in the impact-parameter plane. In Fig. 8, we have shown the $\tilde{A}_{1,0}(-t) = 2S_z^q(-t)$. Similar to Eq. (5.9) and Eq. (5.10), the quark OAM L_z^q and spin-orbit correlation C_z^q can also be defined with respect to momentum transfer $-t$. The results are presented in Fig. 10 for both the iso-vector and iso-scalar cases. The bands

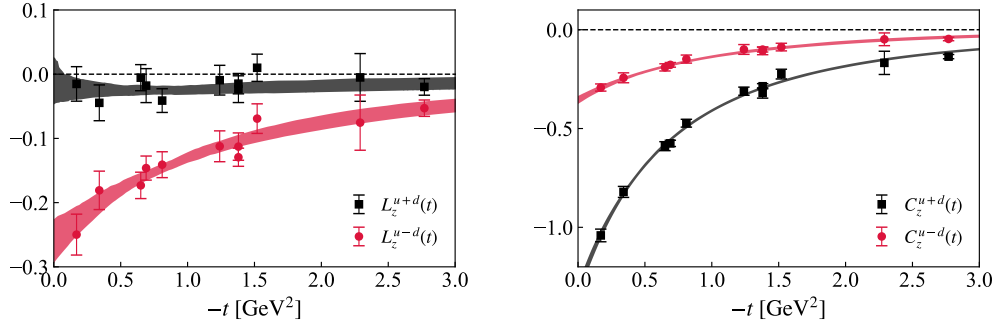


Figure 10. $L_z^q(-t)$ (left panel) and $C_z^q(-t)$ (right panel) are shown as a function of $-t$ for both the iso-vector and iso-scalar cases. The bands are derived from the dipole model fitted from the moments $\tilde{A}_{n,0}(-t)$.

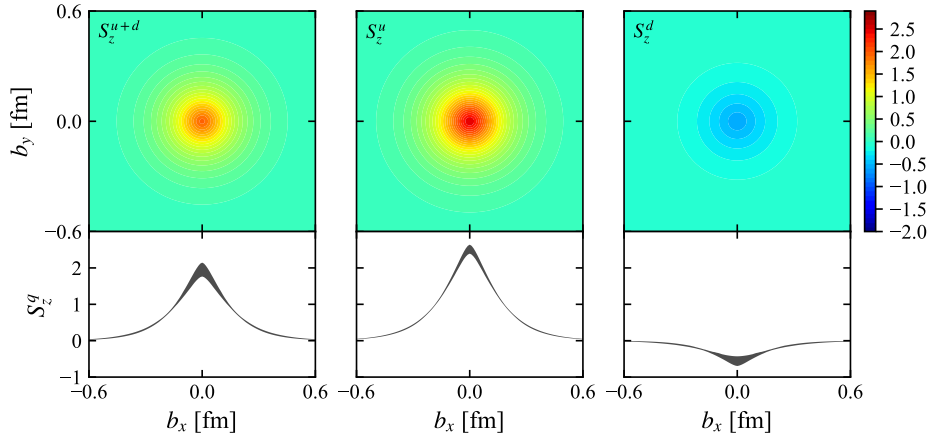


Figure 11. Upper panels: the light quark helicity density in the impact-parameter plane. Lower panels: the light quark helicity density as a function of b_x with $b_y = 0$, including its uncertainties.

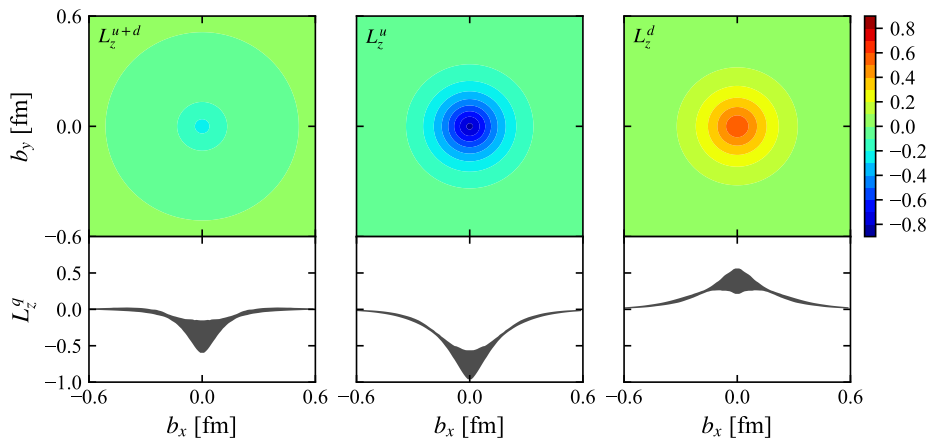


Figure 12. Upper panels: the light quark OAM density in the impact-parameter plane. Lower panels: the light quark OAM density as a function of b_x with $b_y = 0$, including its uncertainties.

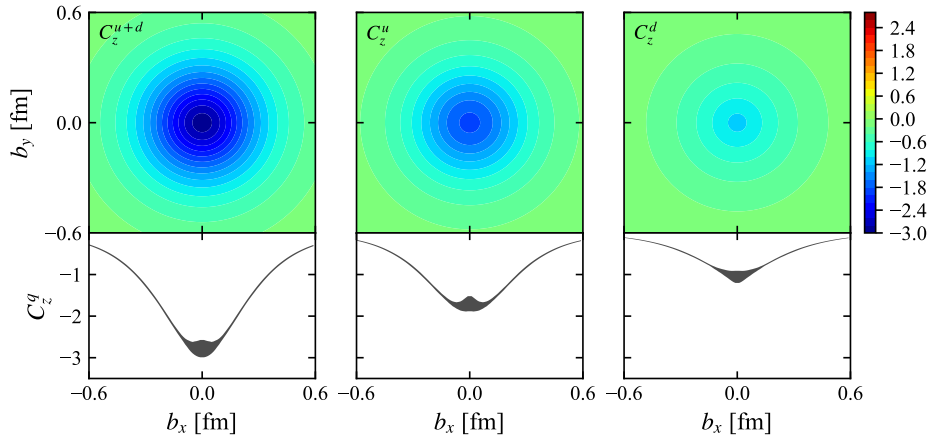


Figure 13. Upper panels: the light quark spin-orbit correlation density in the impact-parameter plane. Lower panels: the light quark spin-orbit correlation density as a function of b_x with $b_y = 0$, including its uncertainties.

are derived using the dipole model fit from Sec. 5.1 by taking the average of the results obtained from the two aforementioned fit ranges. As shown in the figures, the total light-quark OAM, L_z^{u+d} , remains small, and the magnitudes of both $L_z^q(-t)$ and $C_z^q(-t)$ decrease rapidly as $-t$ increases. For the Fourier transform over $-t$, we rely on the fit results from the dipole model, as no data are available beyond 3 GeV^2 . The results at small b_T may be affected by systematic errors due to the model assumptions, though these errors are likely minimal since the moments decay quickly at large $-t$.

In Fig. 11, the quark helicity density in the impact-parameter plane is depicted. As one can see, the u and d quark densities have opposite signs, but the u quark's magnitude is significantly larger, resulting in a positive combined helicity contribution from $u + d$ quarks.

The quark OAM density in the impact-parameter plane, shown in Fig. 12, also exhibits opposite signs for u and d quarks. This suggests that u and d quarks orbit the longitudinal momentum in opposite directions. Notably, since the magnitudes of u and d quarks are similar, their sum is nearly zero. This observation is very different from the quark number density distribution we studied in Ref. [94], where the d quark shows lower magnitudes in the impact-parameter space compared to the u quark. This difference may imply that d quarks possess a larger k_T for a given b_T .

Lastly, for the first time, we present results for the quark spin-orbit correlation distribution in impact-parameter space. We find that these correlations are negative for both light quarks, with the u quark exhibiting a larger magnitude. Interestingly, the sign of $C_z^q = \langle \mathbf{S}_z^q \mathbf{L}_z^q \rangle$ matches that of $S_z^q \cdot L_z^q = \langle \mathbf{S}_z^q \mathbf{S}_z^N \rangle \cdot \langle \mathbf{L}_z^q \mathbf{S}_z^N \rangle$ for each quark flavor. Additionally, unlike S^q and L^q , which approach zero rapidly as b_T nears the nucleon size, there is still a non-zero value observed for the spin-orbit correlation.

6 Conclusion

In this work, we present a study of the moments of axial-vector GPD \tilde{H} using lattice QCD. We compute the quasi-GPD matrix elements in an asymmetric frame with multiple values of the momentum transfer, allowing us to study the t dependence. The quasi-GPDs matrix elements are then renormalized using the ratio scheme. We employ the short-distance factorization framework to extract the first few moments of the GPDs. For the first time, we obtain results for up to and including the fifth moment of axial-vector GPD \tilde{H} with reasonable signal and t dependence as summarized in Table 3 and Table 4. Our determination of the first two moments is consistent with previous calculations using traditional local operator methods. From these moments we infer the quark helicity and OAM contributions to the nucleon spin as well as the quark spin-orbit correlations. In agreement with previous findings, our results indicate that the light quark helicity contributes significantly to the nucleon spin, while the OAM of individual quark flavors shows an interesting pattern of cancellation, leading to a small net OAM for the light quarks. Additionally, the spin-orbit correlations for both light quarks are found to be negative, aligning with the sign of $S_z^q \cdot L_z^q$. The magnitudes of the iso-vector and iso-scalar combinations are in agreement with the large- N_c predictions. We emphasize that the use of an asymmetric frame with multiple values of t enables us to explore impact-parameter space distributions via a Fourier transform over t . That provides us multiple images of the nucleon spin structure, showcasing the spatial distributions of quark helicity, orbital angular momentum (OAM) and, for the first time, the spin-orbit correlations in the transverse plane. These distributions exhibit distinct features for different quark flavors, offering a deeper understanding of the nucleon's internal structure. However, we acknowledge several systematic uncertainties that were not addressed in this exploratory work. Future research will aim to control these uncertainties, including contributions from disconnected diagrams and gluon mixing in the iso-scalar case. It will also involve a careful analysis of excited-state contamination with multiple source-sink separations, calculations with quark masses at the physical point, and the use of multiple lattice spacings to achieve the continuum limit. These efforts aim to further refine our understanding of nucleon spin dynamics.

Acknowledgement

This material is based upon work supported by the U.S. Department of Energy, Office of Science, Office of Nuclear Physics through Contract No. DE-SC0012704, No. DE-AC02-06CH11357 and within the framework of Scientific Discovery through Advance Computing (SciDAC) award Fundamental Nuclear Physics at the Exascale and Beyond. The work of S. B. has been supported by the Laboratory Directed Research and Development program of Los Alamos National Laboratory under project number 20240738PRD1. S. B. has also received support from the U. S. Department of Energy through the Los Alamos National Laboratory. Los Alamos National Laboratory is operated by Triad National Security, LLC, for the National Nuclear Security Administration of U. S. Department of Energy (Contract No. 89233218CNA000001). K. C. is supported by the National Science Centre (Poland)

$-t \text{ GeV}^2$	\tilde{A}_{10}^{u-d}	\tilde{A}_{20}^{u-d}	\tilde{A}_{30}^{u-d}	\tilde{A}_{40}^{u-d}	\tilde{A}_{50}^{u-d}
0.17	0.990(47)(01)	0.262(14)(05)	0.091(05)(01)	0.046(03)(07)	0.017(02)(02)
0.34	0.827(45)(01)	0.215(11)(06)	0.094(05)(01)	0.044(03)(08)	0.022(03)(02)
0.65	0.733(32)(01)	0.223(11)(05)	0.077(04)(01)	0.041(02)(07)	0.015(02)(02)
0.69	0.699(27)(02)	0.221(08)(05)	0.076(04)(02)	0.039(02)(06)	0.016(02)(03)
0.81	0.609(31)(01)	0.192(10)(05)	0.074(04)(01)	0.039(03)(07)	0.019(02)(02)
1.24	0.491(33)(04)	0.159(10)(04)	0.065(06)(04)	0.033(03)(06)	0.020(03)(06)
1.38	0.485(29)(02)	0.181(13)(04)	0.062(05)(02)	0.034(04)(05)	0.012(03)(03)
1.38	0.502(20)(01)	0.173(09)(03)	0.061(03)(01)	0.034(02)(04)	0.010(02)(02)
1.52	0.351(32)(02)	0.143(10)(04)	0.051(05)(02)	0.028(03)(05)	0.014(03)(03)
2.29	0.348(63)(04)	0.161(30)(04)	0.041(10)(04)	0.035(07)(05)	0.006(06)(05)
2.77	0.274(21)(02)	0.119(07)(02)	0.043(04)(02)	0.023(02)(03)	0.006(05)(02)

Table 3. The table of iso-vector moments $\tilde{A}_{n+1,0}^{u-d}$.

$-t \text{ GeV}^2$	\tilde{A}_{10}^{u+d}	\tilde{A}_{20}^{u+d}	\tilde{A}_{30}^{u+d}	\tilde{A}_{40}^{u+d}	\tilde{A}_{50}^{u+d}
0.17	0.554(34)(03)	0.184(07)(05)	0.072(04)(03)	0.036(03)(06)	0.016(02)(03)
0.34	0.531(40)(02)	0.150(13)(04)	0.075(05)(02)	0.032(03)(06)	0.020(03)(03)
0.65	0.427(29)(02)	0.162(07)(04)	0.065(04)(02)	0.032(02)(06)	0.014(02)(02)
0.69	0.424(20)(01)	0.157(07)(05)	0.053(04)(01)	0.033(02)(06)	0.010(02)(01)
0.81	0.407(33)(01)	0.147(10)(04)	0.062(04)(01)	0.030(02)(06)	0.016(03)(02)
1.24	0.296(35)(02)	0.113(11)(03)	0.057(05)(02)	0.025(04)(04)	0.013(03)(03)
1.38	0.313(32)(02)	0.135(10)(03)	0.047(06)(02)	0.028(03)(04)	0.008(03)(02)
1.38	0.290(20)(01)	0.119(07)(03)	0.047(04)(01)	0.026(02)(04)	0.009(02)(02)
1.52	0.217(28)(02)	0.118(09)(03)	0.043(06)(02)	0.022(03)(04)	0.013(03)(02)
2.29	0.231(61)(04)	0.121(24)(05)	0.033(09)(04)	0.030(07)(07)	0.002(07)(05)
2.77	0.199(16)(02)	0.077(07)(03)	0.036(04)(02)	0.018(02)(03)	0.004(02)(02)

Table 4. The table of iso-scalar moments $\tilde{A}_{n+1,0}^{u+d}$.

grants SONATA BIS no. 2016/22/E/ST2/00013 and OPUS no. 2021/43/B/ST2/00497. M. C. and J. M. acknowledge financial support by the U.S. Department of Energy, Office of Nuclear Physics, Early Career Award under Grant No. DE-SC0020405, as well as Grant No. DE-SC0025218. The work of A. M. is supported by the National Science Foundation under grant number PHY-2412792. F. S. was funded by the NSFC and the Deutsche Forschungsgemeinschaft (DFG, German Research Foundation) through the funds provided to the Sino-German Collaborative Research Center TRR110 ‘‘Symmetries and the Emergence of Structure in QCD’’ (NSFC Grant No. 12070131001, DFG Project-ID 196253076 - TRR 110). The authors also acknowledge partial support by the U.S. Department of Energy, Office of Science, Office of Nuclear Physics under the umbrella of the Quark-Gluon Tomography (QGT) Topical Collaboration with Award DE-SC0023646. Computations for this work were carried out in part on facilities of the USQCD Collaboration, which are funded by the Office of Science of the U.S. Department of Energy. This research used

resources of the Oak Ridge Leadership Computing Facility, which is a DOE Office of Science User Facility supported under Contract DE-AC05-00OR22725. This research used resources of the National Energy Research Scientific Computing Center, a DOE Office of Science User Facility supported by the Office of Science of the U.S. Department of Energy under Contract No. DE-AC02-05CH11231 using NERSC award NP-ERCAP0027642. This research was supported in part by PLGrid Infrastructure (Prometheus supercomputer at AGH Cyfronet in Cracow). Computations were also partially performed at the Poznan Supercomputing and Networking Center (Eagle supercomputer), the Interdisciplinary Centre for Mathematical and Computational Modelling of the Warsaw University (Okeanos supercomputer), and at the Academic Computer Centre in Gdańsk (Tryton supercomputer). The gauge configurations have been generated by the Extended Twisted Mass Collaboration on the KNL (A2) Partition of Marconi at CINECA, through the Prace project Pra13.3304 “SIMPHYS”. Inversions were performed using the DD- α AMG solver [127] with twisted mass support [128].

References

- [1] D. Müller, D. Robaschik, B. Geyer, F. M. Dittes, and J. Hořejši, *Wave functions, evolution equations and evolution kernels from light ray operators of QCD*, Fortsch. Phys. **42** (1994) 101–141, [[hep-ph/9812448](#)].
- [2] X.-D. Ji, *Gauge-Invariant Decomposition of Nucleon Spin*, Phys. Rev. Lett. **78** (1997) 610–613, [[hep-ph/9603249](#)].
- [3] A. V. Radyushkin, *Scaling limit of deeply virtual Compton scattering*, Phys. Lett. B **380** (1996) 417–425, [[hep-ph/9604317](#)].
- [4] M. Burkardt, *Impact parameter dependent parton distributions and off forward parton distributions for zeta $\rightarrow 0$* , Phys. Rev. D **62** (2000) 071503, [[hep-ph/0005108](#)]. [Erratum: Phys.Rev.D 66, 119903 (2002)].
- [5] J. P. Ralston and B. Pire, *Femtophotography of protons to nuclei with deeply virtual Compton scattering*, Phys. Rev. D **66** (2002) 111501, [[hep-ph/0110075](#)].
- [6] M. Diehl, *Generalized parton distributions in impact parameter space*, Eur. Phys. J. C **25** (2002) 223–232, [[hep-ph/0205208](#)]. [Erratum: Eur.Phys.J.C 31, 277–278 (2003)].
- [7] M. Burkardt, *Impact parameter space interpretation for generalized parton distributions*, Int. J. Mod. Phys. A **18** (2003) 173–208, [[hep-ph/0207047](#)].
- [8] M. Diehl, *Generalized parton distributions*, Phys. Rept. **388** (2003) 41–277, [[hep-ph/0307382](#)].
- [9] X. Ji, *Generalized parton distributions*, Ann. Rev. Nucl. Part. Sci. **54** (2004) 413–450.
- [10] A. V. Belitsky and A. V. Radyushkin, *Unraveling hadron structure with generalized parton distributions*, Phys. Rept. **418** (2005) 1–387, [[hep-ph/0504030](#)].
- [11] S. Boffi and B. Pasquini, *Generalized parton distributions and the structure of the nucleon*, Riv. Nuovo Cim. **30** (2007), no. 9 387–448, [[arXiv:0711.2625](#)].
- [12] D. Mueller, *Generalized Parton Distributions – visions, basics, and realities –*, Few Body Syst. **55** (2014) 317–337, [[arXiv:1405.2817](#)].

- [13] K. Kumericki, S. Liuti, and H. Moutarde, *GPD phenomenology and DVCS fitting: Entering the high-precision era*, Eur. Phys. J. A **52** (2016), no. 6 157, [[arXiv:1602.02763](#)].
- [14] **European Muon** Collaboration, J. Ashman et al., *A Measurement of the Spin Asymmetry and Determination of the Structure Function $g(1)$ in Deep Inelastic Muon-Proton Scattering*, Phys. Lett. B **206** (1988) 364.
- [15] **European Muon** Collaboration, J. Ashman et al., *An Investigation of the Spin Structure of the Proton in Deep Inelastic Scattering of Polarized Muons on Polarized Protons*, Nucl. Phys. B **328** (1989) 1.
- [16] C. Lorcé, *Spin-orbit correlations in the nucleon*, Phys. Lett. B **735** (2014) 344–348, [[arXiv:1401.7784](#)].
- [17] A. Rajan, M. Engelhardt, and S. Liuti, *Lorentz Invariance and QCD Equation of Motion Relations for Generalized Parton Distributions and the Dynamical Origin of Proton Orbital Angular Momentum*, Phys. Rev. D **98** (2018), no. 7 074022, [[arXiv:1709.05770](#)].
- [18] M. Rodekamp, M. Engelhardt, J. R. Green, S. Krieg, S. Liuti, S. Meinel, J. W. Negele, A. Pochinsky, and S. Syritsyn, *Moments of nucleon unpolarized, polarized, and transversity parton distribution functions from lattice QCD at the physical point*, Phys. Rev. D **109** (2024), no. 7 074508, [[arXiv:2401.05360](#)].
- [19] D. Müller, D. Robaschik, B. Geyer, F. M. Dittes, and J. Hořejši, *Wave functions, evolution equations and evolution kernels from light ray operators of QCD*, Fortsch. Phys. **42** (1994) 101–141, [[hep-ph/9812448](#)].
- [20] X.-D. Ji, *Deeply virtual Compton scattering*, Phys. Rev. D **55** (1997) 7114–7125, [[hep-ph/9609381](#)].
- [21] J. C. Collins and A. Freund, *Proof of factorization for deeply virtual Compton scattering in QCD*, Phys. Rev. D **59** (1999) 074009, [[hep-ph/9801262](#)].
- [22] A. V. Radyushkin, *Asymmetric gluon distributions and hard diffractive electroproduction*, Phys. Lett. B **385** (1996) 333–342, [[hep-ph/9605431](#)].
- [23] J. C. Collins, L. Frankfurt, and M. Strikman, *Factorization for hard exclusive electroproduction of mesons in QCD*, Phys. Rev. D **56** (1997) 2982–3006, [[hep-ph/9611433](#)].
- [24] L. Mankiewicz, G. Piller, and T. Weigl, *Hard exclusive meson production and nonforward parton distributions*, Eur. Phys. J. C **5** (1998) 119–128, [[hep-ph/9711227](#)].
- [25] A. Pedrak, B. Pire, L. Szymanowski, and J. Wagner, *Hard photoproduction of a diphoton with a large invariant mass*, Phys. Rev. D **96** (2017), no. 7 074008, [[arXiv:1708.01043](#)]. [Erratum: Phys.Rev.D 100, 039901 (2019)].
- [26] G. Duplančić, K. Passek-Kumerički, B. Pire, L. Szymanowski, and S. Wallon, *Probing axial quark generalized parton distributions through exclusive photoproduction of a $\gamma\pi^\pm$ pair with a large invariant mass*, JHEP **11** (2018) 179, [[arXiv:1809.08104](#)].
- [27] J.-W. Qiu and Z. Yu, *Exclusive production of a pair of high transverse momentum photons in pion-nucleon collisions for extracting generalized parton distributions*, JHEP **08** (2022) 103, [[arXiv:2205.07846](#)].
- [28] J.-W. Qiu and Z. Yu, *Single diffractive hard exclusive processes for the study of generalized parton distributions*, Phys. Rev. D **107** (2023), no. 1 014007, [[arXiv:2210.07995](#)].

- [29] G. Duplančić, S. Nabeebaccus, K. Passek-Kumerički, B. Pire, L. Szymanowski, and S. Wallon, *Probing chiral-even and chiral-odd leading twist quark generalized parton distributions through the exclusive photoproduction of a $\gamma\rho$ pair*, Phys. Rev. D **107** (2023), no. 9 094023, [[arXiv:2302.12026](#)].
- [30] J.-W. Qiu and Z. Yu, *Extraction of the Parton Momentum-Fraction Dependence of Generalized Parton Distributions from Exclusive Photoproduction*, Phys. Rev. Lett. **131** (2023), no. 16 161902, [[arXiv:2305.15397](#)].
- [31] V. Bertone, H. Dutrieux, C. Mezrag, H. Moutarde, and P. Sznajder, *Deconvolution problem of deeply virtual Compton scattering*, Phys. Rev. D **103** (2021), no. 11 114019, [[arXiv:2104.03836](#)].
- [32] E. Moffat, A. Freese, I. Cloët, T. Donohoe, L. Gamberg, W. Melnitchouk, A. Metz, A. Prokudin, and N. Sato, *Shedding light on shadow generalized parton distributions*, Phys. Rev. D **108** (2023), no. 3 036027, [[arXiv:2303.12006](#)].
- [33] M. Čuić, K. Kumerički, and A. Schäfer, *Separation of Quark Flavors Using Deeply Virtual Compton Scattering Data*, Phys. Rev. Lett. **125** (2020), no. 23 232005, [[arXiv:2007.00029](#)].
- [34] B. Kriesten, P. Velie, E. Yeats, F. Y. Lopez, and S. Liuti, *Parametrization of quark and gluon generalized parton distributions in a dynamical framework*, Phys. Rev. D **105** (2022), no. 5 056022, [[arXiv:2101.01826](#)].
- [35] H. Hashamipour, M. Goharipour, K. Azizi, and S. V. Goloskokov, *Determination of the generalized parton distributions through the analysis of the world electron scattering data considering two-photon exchange corrections*, Phys. Rev. D **105** (2022), no. 5 054002, [[arXiv:2111.02030](#)].
- [36] Y. Guo, X. Ji, and K. Shiells, *Generalized parton distributions through universal moment parameterization: zero skewness case*, JHEP **09** (2022) 215, [[arXiv:2207.05768](#)].
- [37] Y. Guo, X. Ji, M. G. Santiago, K. Shiells, and J. Yang, *Generalized parton distributions through universal moment parameterization: non-zero skewness case*, JHEP **05** (2023) 150, [[arXiv:2302.07279](#)].
- [38] H. Hashamipour, M. Goharipour, K. Azizi, and S. V. Goloskokov, *Generalized parton distributions at zero skewness*, Phys. Rev. D **107** (2023), no. 9 096005, [[arXiv:2211.09522](#)].
- [39] F. Irani, M. Goharipour, H. Hashamipour, and K. Azizi, *Impact of recent MINERvA measurement of the antineutrino-proton scattering cross section on the generalized parton distributions*, Phys. Rev. D **108** (2023), no. 7 074018, [[arXiv:2306.13060](#)].
- [40] M. Čuić, G. Duplančić, K. Kumerički, and K. Passek-K., *NLO corrections to the deeply virtual meson production revisited: impact on the extraction of generalized parton distributions*, JHEP **12** (2023) 192, [[arXiv:2310.13837](#)]. [Erratum: JHEP 02, 225 (2024)].
- [41] **LHPC, SESAM** Collaboration, P. Hagler, J. W. Negele, D. B. Renner, W. Schroers, T. Lippert, and K. Schilling, *Moments of nucleon generalized parton distributions in lattice QCD*, Phys. Rev. D **68** (2003) 034505, [[hep-lat/0304018](#)].
- [42] **QCDSF-UKQCD** Collaboration, D. Brommel et al., *Moments of generalized parton distributions and quark angular momentum of the nucleon*, PoS LATTICE2007 (2007) 158, [[arXiv:0710.1534](#)].
- [43] C. Alexandrou, J. Carbonell, M. Constantinou, P. A. Harraud, P. Guichon, K. Jansen,

- C. Kallidonis, T. Korzec, and M. Papinutto, *Moments of nucleon generalized parton distributions from lattice QCD*, Phys. Rev. D **83** (2011) 114513, [[arXiv:1104.1600](#)].
- [44] C. Alexandrou, M. Constantinou, S. Dinter, V. Drach, K. Jansen, C. Kallidonis, and G. Koutsou, *Nucleon form factors and moments of generalized parton distributions using $N_f = 2 + 1 + 1$ twisted mass fermions*, Phys. Rev. D **88** (2013), no. 1 014509, [[arXiv:1303.5979](#)].
- [45] M. Constantinou, *Hadron Structure*, PoS LATTICE2014 (2015) 001, [[arXiv:1411.0078](#)].
- [46] J. R. Green, J. W. Negele, A. V. Pochinsky, S. N. Syritsyn, M. Engelhardt, and S. Krieg, *Nucleon electromagnetic form factors from lattice QCD using a nearly physical pion mass*, Phys. Rev. D **90** (2014) 074507, [[arXiv:1404.4029](#)].
- [47] C. Alexandrou, M. Constantinou, K. Hadjiyiannakou, K. Jansen, C. Kallidonis, G. Koutsou, and A. Vaquero Aviles-Casco, *Nucleon electromagnetic form factors using lattice simulations at the physical point*, Phys. Rev. D **96** (2017), no. 3 034503, [[arXiv:1706.00469](#)].
- [48] C. Alexandrou, M. Constantinou, K. Hadjiyiannakou, K. Jansen, C. Kallidonis, G. Koutsou, and A. Vaquero Aviles-Casco, *Nucleon axial form factors using $N_f = 2$ twisted mass fermions with a physical value of the pion mass*, Phys. Rev. D **96** (2017), no. 5 054507, [[arXiv:1705.03399](#)].
- [49] N. Hasan, J. Green, S. Meinel, M. Engelhardt, S. Krieg, J. Negele, A. Pochinsky, and S. Syritsyn, *Computing the nucleon charge and axial radii directly at $Q^2 = 0$ in lattice QCD*, Phys. Rev. D **97** (2018), no. 3 034504, [[arXiv:1711.11385](#)].
- [50] R. Gupta, Y.-C. Jang, H.-W. Lin, B. Yoon, and T. Bhattacharya, *Axial Vector Form Factors of the Nucleon from Lattice QCD*, Phys. Rev. D **96** (2017), no. 11 114503, [[arXiv:1705.06834](#)].
- [51] S. Capitani, M. Della Morte, D. Djukanovic, G. M. von Hippel, J. Hua, B. Jäger, P. M. Junnarkar, H. B. Meyer, T. D. Rae, and H. Wittig, *Isvector axial form factors of the nucleon in two-flavor lattice QCD*, Int. J. Mod. Phys. A **34** (2019), no. 02 1950009, [[arXiv:1705.06186](#)].
- [52] C. Alexandrou, S. Bacchio, M. Constantinou, J. Finkenrath, K. Hadjiyiannakou, K. Jansen, G. Koutsou, and A. Vaquero Aviles-Casco, *Proton and neutron electromagnetic form factors from lattice QCD*, Phys. Rev. D **100** (2019), no. 1 014509, [[arXiv:1812.10311](#)].
- [53] E. Shintani, K.-I. Ishikawa, Y. Kuramashi, S. Sasaki, and T. Yamazaki, *Nucleon form factors and root-mean-square radii on a $(10.8 \text{ fm})^4$ lattice at the physical point*, Phys. Rev. D **99** (2019), no. 1 014510, [[arXiv:1811.07292](#)]. [Erratum: Phys.Rev.D 102, 019902 (2020)].
- [54] G. S. Bali, S. Collins, M. Gruber, A. Schäfer, P. Wein, and T. Wurm, *Solving the PCAC puzzle for nucleon axial and pseudoscalar form factors*, Phys. Lett. B **789** (2019) 666–674, [[arXiv:1810.05569](#)].
- [55] G. S. Bali, S. Collins, M. Göckeler, R. Rödl, A. Schäfer, and A. Sternbeck, *Nucleon generalized form factors from two-flavor lattice QCD*, Phys. Rev. D **100** (2019), no. 1 014507, [[arXiv:1812.08256](#)].
- [56] C. Alexandrou et al., *Moments of nucleon generalized parton distributions from lattice QCD*

- simulations at physical pion mass*, Phys. Rev. D **101** (2020), no. 3 034519, [[arXiv:1908.10706](#)].
- [57] Y.-C. Jang, R. Gupta, H.-W. Lin, B. Yoon, and T. Bhattacharya, *Nucleon electromagnetic form factors in the continuum limit from $(2+1+1)$ -flavor lattice QCD*, Phys. Rev. D **101** (2020), no. 1 014507, [[arXiv:1906.07217](#)].
- [58] M. Constantinou et al., *Parton distributions and lattice-QCD calculations: Toward 3D structure*, Prog. Part. Nucl. Phys. **121** (2021) 103908, [[arXiv:2006.08636](#)].
- [59] C. Alexandrou et al., *Moments of the nucleon transverse quark spin densities using lattice QCD*, Phys. Rev. D **107** (2023), no. 5 054504, [[arXiv:2202.09871](#)].
- [60] **Precision Neutron Decay Matrix Elements (PNDME) Collaboration**, Y.-C. Jang, R. Gupta, T. Bhattacharya, B. Yoon, and H.-W. Lin, *Nucleon isovector axial form factors*, Phys. Rev. D **109** (2024), no. 1 014503, [[arXiv:2305.11330](#)].
- [61] A. Shindler, *Moments of parton distribution functions of any order from lattice QCD*, [[arXiv:2311.18704](#)].
- [62] C. Monahan and K. Orginos, *Quasi parton distributions and the gradient flow*, JHEP **03** (2017) 116, [[arXiv:1612.01584](#)].
- [63] Z. Davoudi and M. J. Savage, *Restoration of Rotational Symmetry in the Continuum Limit of Lattice Field Theories*, Phys. Rev. D **86** (2012) 054505, [[arXiv:1204.4146](#)].
- [64] K.-F. Liu and S.-J. Dong, *Origin of difference between anti-d and anti-u partons in the nucleon*, Phys. Rev. Lett. **72** (1994) 1790–1793, [[hep-ph/9306299](#)].
- [65] U. Aglietti, M. Ciuchini, G. Corbo, E. Franco, G. Martinelli, and L. Silvestrini, *Model independent determination of the light cone wave functions for exclusive processes*, Phys. Lett. **B441** (1998) 371–375, [[hep-ph/9806277](#)].
- [66] W. Detmold and C. J. D. Lin, *Deep-inelastic scattering and the operator product expansion in lattice QCD*, Phys. Rev. **D73** (2006) 014501, [[hep-lat/0507007](#)].
- [67] V. Braun and D. Müller, *Exclusive processes in position space and the pion distribution amplitude*, Eur. Phys. J. C **55** (2008) 349–361, [[arXiv:0709.1348](#)].
- [68] X. Ji, *Parton Physics on a Euclidean Lattice*, Phys. Rev. Lett. **110** (2013) 262002, [[arXiv:1305.1539](#)].
- [69] X. Ji, *Parton Physics from Large-Momentum Effective Field Theory*, Sci. China Phys. Mech. Astron. **57** (2014) 1407–1412, [[arXiv:1404.6680](#)].
- [70] A. J. Chambers et al., *Nucleon Structure Functions from Operator Product Expansion on the Lattice*, Phys. Rev. Lett. **118** (2017), no. 24 242001, [[arXiv:1703.01153](#)].
- [71] A. V. Radyushkin, *Quasi-parton distribution functions, momentum distributions, and pseudo-parton distribution functions*, Phys. Rev. D **96** (2017), no. 3 034025, [[arXiv:1705.01488](#)].
- [72] K. Orginos, A. Radyushkin, J. Karpie, and S. Zafeiropoulos, *Lattice QCD exploration of parton pseudo-distribution functions*, Phys. Rev. **D96** (2017), no. 9 094503, [[arXiv:1706.05373](#)].
- [73] Y.-Q. Ma and J.-W. Qiu, *Extracting Parton Distribution Functions from Lattice QCD Calculations*, Phys. Rev. **D98** (2018), no. 7 074021, [[arXiv:1404.6860](#)].

- [74] **HOPE** Collaboration, W. Detmold, A. V. Grebe, I. Kanamori, C. J. D. Lin, R. J. Perry, and Y. Zhao, *Parton physics from a heavy-quark operator product expansion: Formalism and Wilson coefficients*, Phys. Rev. D **104** (2021), no. 7 074511, [[arXiv:2103.09529](#)].
- [75] X. Gao, W.-Y. Liu, and Y. Zhao, *Parton distributions from boosted fields in the Coulomb gauge*, Phys. Rev. D **109** (2024), no. 9 094506, [[arXiv:2306.14960](#)].
- [76] X. Ji, Y.-S. Liu, Y. Liu, J.-H. Zhang, and Y. Zhao, *Large-momentum effective theory*, Rev. Mod. Phys. **93** (2021), no. 3 035005, [[arXiv:2004.03543](#)].
- [77] K. Cichy and M. Constantinou, *A guide to light-cone PDFs from Lattice QCD: an overview of approaches, techniques and results*, Adv. High Energy Phys. **2019** (2019) 3036904, [[arXiv:1811.07248](#)].
- [78] M. Constantinou, *The x -dependence of hadronic parton distributions: A review on the progress of lattice QCD*, Eur. Phys. J. A **57** (2021), no. 2 77, [[arXiv:2010.02445](#)].
- [79] K. Cichy, *Progress in x -dependent partonic distributions from lattice QCD*, PoS LATTICE2021 (2022) 017, [[arXiv:2110.07440](#)].
- [80] K. Cichy, *Overview of lattice calculations of the x -dependence of PDFs, GPDs and TMDs*, EPJ Web Conf. **258** (2022) 01005, [[arXiv:2111.04552](#)].
- [81] X. Gao, *Overview of hadron structure form lattice QCD*, PoS LATTICE2023 (2024) 128.
- [82] J. Karpie, K. Orginos, and S. Zafeiropoulos, *Moments of Ioffe time parton distribution functions from non-local matrix elements*, JHEP **11** (2018) 178, [[arXiv:1807.10933](#)].
- [83] J.-W. Chen, H.-W. Lin, and J.-H. Zhang, *Pion generalized parton distribution from lattice QCD*, Nucl. Phys. B **952** (2020) 114940, [[arXiv:1904.12376](#)].
- [84] C. Alexandrou, K. Cichy, M. Constantinou, K. Hadjiyiannakou, K. Jansen, A. Scapellato, and F. Steffens, *Unpolarized and helicity generalized parton distributions of the proton within lattice QCD*, Phys. Rev. Lett. **125** (2020), no. 26 262001, [[arXiv:2008.10573](#)].
- [85] H.-W. Lin, *Nucleon Tomography and Generalized Parton Distribution at Physical Pion Mass from Lattice QCD*, Phys. Rev. Lett. **127** (2021), no. 18 182001, [[arXiv:2008.12474](#)].
- [86] C. Alexandrou, K. Cichy, M. Constantinou, K. Hadjiyiannakou, K. Jansen, A. Scapellato, and F. Steffens, *Transversity GPDs of the proton from lattice QCD*, Phys. Rev. D **105** (2022), no. 3 034501, [[arXiv:2108.10789](#)].
- [87] **CSSM/QCDSF/UKQCD** Collaboration, A. Hannaford-Gunn, K. U. Can, R. Horsley, Y. Nakamura, H. Perlt, P. E. L. Rakow, H. Stüben, G. Schierholz, R. D. Young, and J. M. Zanotti, *Generalized parton distributions from the off-forward Compton amplitude in lattice QCD*, Phys. Rev. D **105** (2022), no. 1 014502, [[arXiv:2110.11532](#)].
- [88] S. Bhattacharya, K. Cichy, M. Constantinou, J. Dodson, A. Metz, A. Scapellato, and F. Steffens, *First Lattice QCD Study of Proton Twist-3 GPDs*, [[arXiv:2112.05538](#)].
- [89] H.-W. Lin, *Nucleon helicity generalized parton distribution at physical pion mass from lattice QCD*, Phys. Lett. B **824** (2022) 136821, [[arXiv:2112.07519](#)].
- [90] S. Bhattacharya, K. Cichy, M. Constantinou, J. Dodson, X. Gao, A. Metz, S. Mukherjee, A. Scapellato, F. Steffens, and Y. Zhao, *Generalized parton distributions from lattice QCD with asymmetric momentum transfer: Unpolarized quarks*, Phys. Rev. D **106** (2022), no. 11 114512, [[arXiv:2209.05373](#)].

- [91] M. Constantinou, S. Bhattacharya, K. Cichy, J. Dodson, X. Gao, A. Metz, S. Mukherjee, A. Scapellato, F. Steffens, and Y. Zhao, *Accessing proton GPDs in asymmetric frames: Numerical implementation*, PoS LATTICE2022 (2023) 096, [[arXiv:2212.09818](#)].
- [92] S. Bhattacharya, K. Cichy, M. Constantinou, J. Dodson, X. Gao, A. Metz, S. Mukherjee, A. Scapellato, F. Steffens, and Y. Zhao, *GPDs in asymmetric frames*, PoS LATTICE2022 (2023) 095, [[arXiv:2301.03400](#)].
- [93] K. Cichy et al., *Generalized Parton Distributions from Lattice QCD*, in 29th Cracow Epiphany Conference, 4, 2023. [arXiv:2304.14970](#).
- [94] S. Bhattacharya, K. Cichy, M. Constantinou, X. Gao, A. Metz, J. Miller, S. Mukherjee, P. Petreczky, F. Steffens, and Y. Zhao, *Moments of proton GPDs from the OPE of nonlocal quark bilinears up to NNLO*, Phys. Rev. D **108** (2023), no. 1 014507, [[arXiv:2305.11117](#)].
- [95] S. Bhattacharya, K. Cichy, M. Constantinou, J. Dodson, A. Metz, A. Scapellato, and F. Steffens, *Chiral-even axial twist-3 GPDs of the proton from lattice QCD*, Phys. Rev. D **108** (2023), no. 5 054501, [[arXiv:2306.05533](#)].
- [96] S. Bhattacharya, K. Cichy, M. Constantinou, A. Metz, N. Nurminen, and F. Steffens, *Generalized parton distributions from the pseudo-distribution approach on the lattice*, [arXiv:2405.04414](#).
- [97] **HadStruc** Collaboration, H. Dutrieux, R. G. Edwards, C. Egerer, J. Karpie, C. Monahan, K. Orginos, A. Radyushkin, D. Richards, E. Romero, and S. Zafeiropoulos, *Towards Unpolarized GPDs from Pseudo-Distributions*, [arXiv:2405.10304](#).
- [98] H.-T. Ding, X. Gao, S. Mukherjee, P. Petreczky, Q. Shi, S. Syritsyn, and Y. Zhao, *Lattice QCD calculation of the pion generalized parton distribution*, PoS SPIN2023 (2024) 024.
- [99] H.-T. Ding, X. Gao, S. Mukherjee, P. Petreczky, Q. Shi, S. Syritsyn, and Y. Zhao, *Three-dimensional Imaging of Pion using Lattice QCD: Generalized Parton Distributions*, [arXiv:2407.03516](#).
- [100] S. Bhattacharya et al., *Generalized parton distributions from lattice QCD with asymmetric momentum transfer: Axial-vector case*, Phys. Rev. D **109** (2024), no. 3 034508, [[arXiv:2310.13114](#)].
- [101] D. V. Kiptily and M. V. Polyakov, *Genuine twist three contributions to the generalized parton distributions from instantons*, Eur. Phys. J. C **37** (2004) 105–114, [[hep-ph/0212372](#)].
- [102] M. Constantinou and H. Panagopoulos, *Perturbative renormalization of quasi-parton distribution functions*, Phys. Rev. D **96** (2017), no. 5 054506, [[arXiv:1705.11193](#)].
- [103] J.-W. Chen, T. Ishikawa, L. Jin, H.-W. Lin, Y.-B. Yang, J.-H. Zhang, and Y. Zhao, *Parton distribution function with nonperturbative renormalization from lattice QCD*, Phys. Rev. D **97** (2018), no. 1 014505, [[arXiv:1706.01295](#)].
- [104] C. Alexandrou et al., *Simulating twisted mass fermions at physical light, strange and charm quark masses*, Phys. Rev. D **98** (2018), no. 5 054518, [[arXiv:1807.00495](#)].
- [105] G. S. Bali, B. Lang, B. U. Musch, and A. Schäfer, *Novel quark smearing for hadrons with high momenta in lattice QCD*, Phys. Rev. D **93** (2016), no. 9 094515, [[arXiv:1602.05525](#)].
- [106] C. Alexandrou, M. Constantinou, K. Hadjiyiannakou, K. Jansen, and F. Manigrasso, *Flavor decomposition of the nucleon unpolarized, helicity, and transversity parton distribution functions from lattice QCD simulations*, Phys. Rev. D **104** (2021), no. 5 054503, [[arXiv:2106.16065](#)].

- [107] **ETM** Collaboration, C. Alexandrou, M. Brinet, J. Carbonell, M. Constantinou, P. A. Harraud, P. Guichon, K. Jansen, T. Korzec, and M. Papinutto, *Axial Nucleon form factors from lattice QCD*, Phys. Rev. D **83** (2011) 045010, [[arXiv:1012.0857](#)].
- [108] X. Ji, J.-H. Zhang, and Y. Zhao, *Renormalization in Large Momentum Effective Theory of Parton Physics*, Phys. Rev. Lett. **120** (2018), no. 11 112001, [[arXiv:1706.08962](#)].
- [109] J. Green, K. Jansen, and F. Steffens, *Nonperturbative Renormalization of Nonlocal Quark Bilinears for Parton Quasidistribution Functions on the Lattice Using an Auxiliary Field*, Phys. Rev. Lett. **121** (2018), no. 2 022004, [[arXiv:1707.07152](#)].
- [110] T. Ishikawa, Y.-Q. Ma, J.-W. Qiu, and S. Yoshida, *Renormalizability of quasiparton distribution functions*, Phys. Rev. D **96** (2017), no. 9 094019, [[arXiv:1707.03107](#)].
- [111] Z. Fan, X. Gao, R. Li, H.-W. Lin, N. Karthik, S. Mukherjee, P. Petreczky, S. Syritsyn, Y.-B. Yang, and R. Zhang, *Isvector parton distribution functions of the proton on a superfine lattice*, Phys. Rev. D **102** (2020), no. 7 074504, [[arXiv:2005.12015](#)].
- [112] X. Gao, L. Jin, C. Kallidonis, N. Karthik, S. Mukherjee, P. Petreczky, C. Shugert, S. Syritsyn, and Y. Zhao, *Valence parton distribution of the pion from lattice QCD: Approaching the continuum limit*, Phys. Rev. D **102** (2020), no. 9 094513, [[arXiv:2007.06590](#)].
- [113] T. Izubuchi, X. Ji, L. Jin, I. W. Stewart, and Y. Zhao, *Factorization Theorem Relating Euclidean and Light-Cone Parton Distributions*, Phys. Rev. D **98** (2018), no. 5 056004, [[arXiv:1801.03917](#)].
- [114] X. Gao, K. Lee, S. Mukherjee, C. Shugert, and Y. Zhao, *Origin and resummation of threshold logarithms in the lattice QCD calculations of PDFs*, Phys. Rev. D **103** (2021), no. 9 094504, [[arXiv:2102.01101](#)].
- [115] Y. Su, J. Holligan, X. Ji, F. Yao, J.-H. Zhang, and R. Zhang, *Resumming quark's longitudinal momentum logarithms in LaMET expansion of lattice PDFs*, Nucl. Phys. B **991** (2023) 116201, [[arXiv:2209.01236](#)].
- [116] **HadStruc** Collaboration, H. Dutrioux, J. Karpie, C. Monahan, K. Orginos, and S. Zafeiropoulos, *Evolution of parton distribution functions in the short-distance factorization scheme*, JHEP **04** (2024) 061, [[arXiv:2310.19926](#)].
- [117] F. Yao, Y. Ji, and J.-H. Zhang, *Connecting Euclidean to light-cone correlations: from flavor nonsinglet in forward kinematics to flavor singlet in non-forward kinematics*, JHEP **11** (2023) 021, [[arXiv:2212.14415](#)].
- [118] A. S. Baran, J. T. Gilker, L. Fox-Machado, M. D. Reed, and S. D. Kawaler, *RAT J0455+1305: A rare hybrid pulsating subdwarf B star*, Mon. Not. Roy. Astron. Soc. **411** (2011) 776, [[arXiv:1103.1600](#)].
- [119] C. Lorce and B. Pasquini, *Quark Wigner Distributions and Orbital Angular Momentum*, Phys. Rev. D **84** (2011) 014015, [[arXiv:1106.0139](#)].
- [120] K. Kanazawa, C. Lorcé, A. Metz, B. Pasquini, and M. Schlegel, *Twist-2 generalized transverse-momentum dependent parton distributions and the spin/orbital structure of the nucleon*, Phys. Rev. D **90** (2014), no. 1 014028, [[arXiv:1403.5226](#)].
- [121] S. Bhattacharya, R. Boussarie, and Y. Hatta, *Spin-orbit entanglement in the Color Glass Condensate*, [arXiv:2404.04208](#).

- [122] S. Bhattacharya, R. Boussarie, and Y. Hatta, *Exploring orbital angular momentum and spin-orbit correlation for gluons at the Electron-Ion Collider*, [arXiv:2404.04209](#).
- [123] Y. Hatta and J. Schoenleber, *Twist analysis of the spin-orbit correlation in QCD*, [arXiv:2404.18872](#).
- [124] G. Lee, J. R. Arrington, and R. J. Hill, *Extraction of the proton radius from electron-proton scattering data*, Phys. Rev. D **92** (2015), no. 1 013013, [[arXiv:1505.01489](#)].
- [125] K.-F. Liu, *Status on lattice calculations of the proton spin decomposition*, AAPPS Bull. **32** (2022), no. 1 8, [[arXiv:2112.08416](#)].
- [126] J.-Y. Kim, H.-Y. Won, H.-C. Kim, and C. Weiss, *Spin-orbit correlations in the nucleon in the large- N_c limit*, [arXiv:2403.07186](#).
- [127] A. Frommer, K. Kahl, S. Krieg, B. Leder, and M. Rottmann, *Adaptive Aggregation Based Domain Decomposition Multigrid for the Lattice Wilson Dirac Operator*, SIAM J. Sci. Comput. **36** (2014) A1581–A1608, [[arXiv:1303.1377](#)].
- [128] C. Alexandrou, S. Bacchio, J. Finkenrath, A. Frommer, K. Kahl, and M. Rottmann, *Adaptive Aggregation-based Domain Decomposition Multigrid for Twisted Mass Fermions*, Phys. Rev. D **94** (2016), no. 11 114509, [[arXiv:1610.02370](#)].